



Chemical
Science

**Magnetic circularly polarized luminescence from spin flip
transitions in a molecular ruby**

Journal:	<i>Chemical Science</i>
Manuscript ID	SC-EDG-07-2024-004718.R1
Manuscript Type:	Edge Article

SCHOLARONE™
Manuscripts

Chemical Science

Guidelines for Referees

Thank you very much for agreeing to review this manuscript for [Chemical Science](#).



Chemical Science is the flagship journal from the Royal Society of Chemistry publishing findings from across the breadth of the chemical sciences.

Articles should be of exceptional significance to their field, which would also be of wider interest to readers working in other areas across the chemical sciences.

For more information about *Chemical Science* please visit [our website here](#).

The following manuscript has been submitted for consideration as an

EDGE ARTICLE

For acceptance, an Edge article must report primary research which provides a significant new concept, advance or insight into the development of its field, and be of interest to scientists across the broad multi-disciplinary readership of the journal. There are no page limits for Edge articles, so authors can choose how best to present their research. However Electronic Supplementary Information (ESI) is recommended for additional data and experimental details.

We ask referees to **recommend only the most significant work** for publication in *Chemical Science*. When making your recommendation please:

- **Comment on** the novelty and significance to the field, the broader appeal and scientific reliability.
- **Note that routine or incremental** work should not be recommended for publication.
- **Contact the Associate Editor** if there is any conflict of interest, if the work has been previously published or if there is a significant part of the work which you are not able to referee with confidence.

PLEASE NOTE: *Chemical Science* offers authors the option of transparent peer review (TPR). If authors choose TPR, the reviewers' comments, authors' response and editor's decision letter for all stages of review are also published if the article is accepted. Reviewers will remain anonymous unless they choose to sign their report and only comments to the authors will be published – confidential comments to the editor will not be published.

Please note by peer reviewing you give consent to your anonymised report being published if authors have selected TPR.

Best regards,

Professor Andrew Cooper

Editor-in-Chief, *Chemical Science*

Dr May Copsey

Executive Editor, *Chemical Science*

Contact us

Please visit our [reviewer hub](#) for further details of our processes, policies and reviewer responsibilities as well as guidance on how to review, or click the links below.



What to do
when you
review



Reviewer
responsibilities



Process &
policies



DIPARTIMENTO DI
CHIMICA E CHIMICA
INDUSTRIALE

Dr. Francesco Zinna

Via Giuseppe Moruzzi, 13
56124 Pisa (Italy)
Tel. + 39 050 2219275
Francesco.zinna@unipi.it

Cod. Fisc. 80003670504
P. IVA 0028682 050 1

Pisa, September 2nd 2024

Dear Prof. Gabbai,

We are submitting a revised version of our manuscript *Magnetic circularly polarized luminescence from spin flip transitions in a molecular Ruby*

We thank the referees for their comments and their overall positive assessment of our work. We believe we have improved the manuscript by clarifying a few points and improving our data analysis.

We attach in the following a point-by-point reply to all referees' comments.

We hope that now the manuscript can be considered acceptable for publication in *Chemical Science*.

Yours sincerely

Referee: 1**Comments:**

It is obviously a brilliant work in photophysical properties of transition metal complexes. Responsiveness of transition metal complexes towards magnetic field is one of the important topics in inorganic chemistry. The salient feature of the current submission are on the data analysis on the magnetic CPL (MCPL) and magnetic CD (MCD) obtained with a spin-flip and phosphorescent Cr(III) complexes. I am not working on the MCPL/MCD spectroscopy, and hence my comments could be general. I suggest the following minor revisions:

(1) The abstract of the current submission is too general and is lack of results and conclusion. The readers cannot grasp the most important data from the abstract.

We have rewritten the abstract to make it clearer and more specific.

(2) Throughout the main text including the figure captions, the reader cannot find how these important MCPL/MCD data were measured. For example, the authors did NOT provide in the main text the information of the solvent used for measurement. The authors failed to provide how the applied magnetic field was continuously tuned from -1.5 T to +1.5 T.

We thank the reviewer for pointing this out. We now have added this information in the captions of Fig. 2 and 3, and in the text at the beginning of the Results section: "Optical and magneto-optical studies reported here were performed on deaerated acetonitrile solutions of the racemic compound ($[\text{Cr}(\text{dqp})_2](\text{PF}_6)_3$)."

The MCPL measurements were reported at constant magnetic field (0.4 T), as our MCPL setup employs a permanent magnet, as specified in the experimental part in the supporting information file. Positive and negative field CPL spectra were acquired by simply reversing the magnet. We have made this explicit in the main text.

In MCD characterization we also performed spectra at different fields, as well as MCD vs field plots. Indeed, MCD setup is equipped with an electromagnet, which is made of two coils and two perforated iron cylinders at a distance of about 5 mm. The sample is placed between the two iron cylinders, where the magnetic field is concentrated. The electromagnet is able to vary the applied field in the range ± 1.4 T, by changing the current passing in the coils. We have now added this information in the experimental part related to MCD, in the supporting information file: "MCD vs field plots in the ± 1.4 T range were also acquired by regulating the current passing in the coils of the electromagnet. The strength of the magnetic field was measured with a Hall probe."

(3) To my knowledge, the MCPL/MCD should be in strict mirror images for an achiral or racemic system under applied S(+) and S(-) magnetic field (BTW, the authors should explain a little more how to define S(+) and S(-)). The authors provided semi-difference MCPL field, aiming to eliminate all the magnetic-independent contributions, such as baseline effects and possible artefact signals due to photoselection. I understand this is possibly a general method for data curation, but the authors should elaborate here to the readers not familiar with the MCPL technique, such as me.

For what concerns the definitions of positive and negative fields, we refer to the standard convention used in MCD spectroscopy, which we know added in the manuscript text: "Positive and negative fields are here defined as parallel and anti-parallel to the k-vector, i.e. the propagating direction of light."

Regarding the elimination of artifacts in MCPL and MCD, it is routinely done by making the semidifference between the signal with positive and negative fields. In this way all the contributions (artefacts) that do not depend on the magnetic field are eliminated in the subtraction. This is a peculiar advantage of magneto-optical techniques, where the signal reverses its sign by reversing the magnetic field. Baseline subtraction is particularly important in MCPL, where the signal is only arising from the sample, thus a blank cuvette would not give any signal. As typical MCPL signal is at least 1 order of magnitude lower than CPL, it is particularly important to clean the signal through the semi-difference between the two fields, as non-perfect alignment of the optical components can give an apparent CPL signals which should have to be subtracted.

We have expanded the text to better explain this concept: "Baseline effects and possible artefact signals due to photoselection, cause some deviation from the mirror image relationship expected for spectra obtained under opposite magnetic field, especially in the case of small signals (Figure S3a). The data treated according to Eq. 2 ensures that such artefacts, which are magnetic field-independent, are eliminated and only the true MCPL is recovered"

Referee: 2**Comments:**

In this manuscript, the authors investigated magnetic circularly polarized luminescence (MCPL) of $[\text{Cr}(\text{dqp})_2]^{3+}$. The electronic structures of this complex were characterized by the UV-vis, magnetic circular dichroism (MCD), MCPL, and high-frequency and -field EPR (HFEPR) spectroscopy. The MCD and MCPL spectra were quantitatively analyzed by a band deconvolution method, and the HFEPR spectra were analyzed based on spin-Hamiltonian of the quartet state. The precise analyses are plausible and useful, and therefore, this manuscript seems to be publishable. However, before accepting this manuscript, the authors should address the following points.

1, The authors described “This confirms that magneto-optical techniques are excellent tools to study SF transitions.”, but the previous papers related to the MCD of SF transitions (ex. European Journal of Inorganic Chemistry, 2017, 5103-5107, 2017. Journal of Physical Chemistry Letters, 11, 9828-9833, 2020.) were not cited. The authors should cite them to clearly show the positioning of this research.

In the introduction, we have added a sentence related to the previous MCD studies mentioned by the reviewer: “MCD was also used to study far red/near infrared (NIR) transitions in the case of Ir or Pt complexes,^{67,68} where their observation through emission, and thus MCPL, is challenging. On the other hand, emissive Cr(III) compounds are potentially a more suitable platform to address metal transitions through MCPL.” The suggested references have been added as well (new refs 67 and 68).

2, In Table S1, the authors analyzed the $^4A_2 \rightarrow ^4T_2$ transitions using the UV-vis and MCD spectroscopy. Firstly, the peaks 1-3 should be explained using zero field splitting and Zeeman splitting like Figure 4 for the general readers. The second is the notation. Does the δ value mean the 1/2 ZFS? What is the meaning of w = peak width? Full Width at Half Maximum? The authors should clarify the notations.

It is true that the fine structure of the ground level due to Zeeman splitting and ZFS splitting play a role in determining the whole shape of the MCD spectrum, which is probably given by C and B terms and possibly higher energy transitions overlapping. As it is not possible here to disentangle all the contributions, the analysis is merely phenomenological, as we do not make assumptions on the origin of the MCD signals, rather we are only interested in the energy barycenters of the $^4A_2 \rightarrow ^4T_2$ transitions. We have tried to make the nature of the analysis clearer. Note that we closely followed the method proposed by van Slaageren et al. reported in a few works for similar complexes (e.g. 10.1039/C9CP00745H, 10.1002/chem.202202898).

We confirm that w is the full width at half maximum of the peak, and we corrected this in the caption of Figure S1, where it is now called σ for consistency. We removed the δ notation, and we corrected a missing “2” factor to describe the full ZFS.

The third is the “Standard Error”. The Standard Error (3112 cm^{-1}) of the energy of peak 1 seems to be much larger than those of peaks 2 and 3, and therefore, it seems to be inappropriate for the detailed analyses. The authors should check them carefully.

We agree that the fitting of peak 1 is affected by a significant error. However, the obtained energies give comparable results in terms of D and E values with respect to HFEPR analysis, which make us confident that the results are reliable.

We have clarified in the text that these results are however approximate and affected by a large error.

3, The authors measured the HFEPR spectra of a polycrystalline sample or a pellet sample, and described “a single crystal oriented with the z-axis of the ZFS tensor parallel to the magnetic field B_0 ”. The review think it is better to investigate the frozen solution of $[Cr(dqp)_2]^{3+}$ as a randomly oriented sample. The authors should examine it.

It is true that a frozen solution can provide a random distribution of molecules relative to the field, but so does a pellet. The main advantage of a solution over a pellet is that it provides magnetic dilution. However, our spectra do not show a need for magnetic dilution as the resonances are crisp and narrow, and show little or no sign of magnetic interactions between the spins. A frozen solution experiment has also drawbacks: (a) the solvent heavily absorbs sub-THz waves reducing the S/N ratio, (b) the solvent needs to form a good low-temperature glass, and (c) most importantly, one needs to achieve sufficient concentration to observe a spectrum. This concentration limit differs from one transition ion to another, but a good guess for Cr(III) in our spectrometer would be at least 10 - 50 mM.

Referee: 3

Comments:

The manuscript reports on the magneto-optical study of the Cr(III) complex, $[Cr(dqp)_2]^{3+}$, with quasi-octahedral coordination. This complex is chiral and well known for its circular-polarized photoluminescence (CPL), but the influence of magnetic field on CPL and spin-flip emission in such complexes has not been studied yet. The authors demonstrate clear magnetochiral response in luminescence and absorption spectra and reconstruct the structure of ground state levels based on these data. High-frequency EPR study is also performed to determine ZFS parameters and to demonstrate the reliability of the parameters determined from M-CPL measurements. I find the work to be well organized and performed, results will be of high interest to the broad audience, and the manuscript can be recommended for publication in Chem Sci. However, I have two questions, which the authors may consider in the revised version.

1. First, in the emitting $2E$ state, the authors consider only the lowest-energy component. It is not very clear why they can ignore the higher-energy components. What is the size of the splitting? What could be thermal populations for that higher state at room temperature?

From the better resolved PL spectrum in Fig. S2, we see a weak band lying around 710 nm (approx. 14100 cm^{-1}), which could be associated to the higher energy component of the 2E state (E is doubly degenerate). This component is well

separated from the main 729 nm one and it is very weak in PL with non-significant associated MCPL. Therefore, it can be ignored in the MCPL analysis. We have clarified this better in the revised text.

2. Second, the scheme in Figure 4 considers two non-interacting Kramers doublets in the ground 4A2 state. However, it is clear from the EPR data (Fig. 5) that there seems to be avoided crossing between the levels in the field of 0.4 T (used in MCPL measurements) and hence considerable mixing. The authors can compute this precisely since they have precise spin Hamiltonian parameters from HFEPR measurements. In the situation of mixing, I doubt that the simple rigid-shift approximation remains valid. I think the authors might analyze this situation more carefully.

We thank the referee for raising this important point. Prompted by this suggestion, we computed the mixing coefficients from EPR data. Indeed, considering for example $B_0 \parallel z$, we see that, while the outer levels have a rather well-defined character of $+1/2$ and $-3/2$ (highest and lowest one respectively), the inner ones are mixtures of $-1/2$ and $+3/2$. We have added two new tables (Table S3, S4) in the SI with the mixing coefficients at 0.4 T, as well as an expansion of the EPR levels at low field (Fig. S11).

This also prompted us to improve the analysis of the MCPL data. In the new analysis, we reduced the free parameters and underlying assumptions to explain the MCPL spectrum. Instead of leaving as free parameter the energies of the four ground state levels, in the analysis of MCPL we have now used HFEPR energy levels at 0.4 T (the new Fig. 4 reflects this change). In the new fitting (Fig. 2) only the asymmetry parameter dA is left free, while σ , areas and energy barycenter of the transitions are fitted according to usual rigid shift procedure.

To the best of our knowledge, there is no literature on the treatment of magneto-optical data in the presence of mixed levels. For this reason, we can only treat transitions between pure levels. We are aware that the mixing will affect the purely polarized character of the transitions, which is one of the requirements of the rigid shift approach. Despite this and despite having reduced the number of free parameters, the MCPL is still reasonably well reproduced (new Fig. 2). The overestimation of the simulation with respect to the experimental data may be explained by considering that the state mixing will somewhat reduce the intensity of the simulated MCPL spectrum. We have added these considerations in the revised text. A more quantitative treatment of the mixing in the MCPL data is beyond the scope of the present work, but we expect to expand on the problem in future works.

Note that the rigid shift requirement that the state splitting of the levels is much smaller than the linewidth is still respected.

Small remarks:

Page 3, the phrase “we followed the method proposed by van Slageren et al. (see ESI).72” I think, the reference number here should be 73, not 72

Table S1: peak width is denoted as σ in the table and w in the footnote

In the section “Analysis of MCPL data” in SI, reference to Figure S5 should be changed to Figure S6.

The first paragraph after eq. S13, correct “Table SX” to “Table S2”

Caption to Figure S8: “field dependence of the magnetization at 2 K (inset)”. “2 K” should be corrected to “2–7 K”.

We have corrected the mistakes. We thank the reviewer for noticing them.

ARTICLE

Magnetic circularly polarized luminescence from spin flip transitions in a molecular Ruby

Received 00th January 20xx,
Accepted 00th January 20xx

DOI: 10.1039/x0xx00000x

Alessio Gabbani,^{a,b} Maxime Poncet,^c Gennaro Pescitelli,^a Laura Carbonaro,^a J. Krzystek,^d Enrique Colacio,^e Claude Piguet,^c Francesco Pineider,^{a,b} Lorenzo Di Bari,^a Juan-Ramón Jiménez*,^e Francesco Zinna*^a

Magnetic circularly polarized luminescence (MCPL), i.e. the possibility of generating circularly polarized luminescence in the presence of a magnetic field in achiral or racemic compounds, is a technique of rising interest. Here we show that the far-red spin-flip (SF) transitions of a molecular Cr(III) complex give intense MCD (magnetic circular dichroism) and in particular MCPL (g_{MCPL} up to $6.3 \cdot 10^{-3} T^{-1}$) even at magnetic fields as low as 0.4 T. Cr(III) doublet states and SF emission are nowadays the object of many investigations, as they may open the way to several applications. Due to their nature, such transitions can be conveniently addressed by MCPL, which strongly depends on the zero field splitting and Zeeman splitting of the involved states. Despite the complexity of the nature of such states and the related photophysics, the obtained MCPL data can be rationalized consistently with the information recovered with more established techniques, such as HFEPR (high-frequency and -field electron paramagnetic resonance). We anticipate that emissive molecular Cr(III) species may be useful in magneto-optical devices, such as magnetic CP-OLEDs.

Introduction

Molecular complexes based on d-metals offer a diverse and intriguing photophysics,¹ with applications ranging from photocatalysis,² optoelectronics,^{3,4} imaging^{5,6} and photodynamic therapy.^{7–9} To understand the often non-trivial photophysics at play, the use of less common spectroscopic techniques may be beneficial. In turn, this is necessary to exploit the full potential of those systems and to give indications for a rational design of the ligands and complexes.

A particularly interesting case is observed when metal-centred excited states differ only by spin configuration with respect to the ground state.¹⁰ Such configurations are called spin-flip (SF) states and they may display sharp phosphorescent transitions (SF-transitions), forbidden by electric transition moment, with lifetimes up to a millisecond. SF luminescence was observed in the case of

V(II)/V(III),^{11–13} Mn(IV),^{14,15} Mo(III),^{16,17} Re(IV),¹⁷ and in particular, remarkable results in terms of emission efficiency were obtained in the case of (pseudo)octahedral Cr(III) complexes.^{18–20} Such complexes show luminescence associated with the doublet states $^2T_1/{}^2E$ (Figure 1) with quantum yields up to 30% with narrow bands in the far red or near infrared region.¹⁸ These features, reminiscent of those of the ruby gemstone, can be obtained in a molecular compound with octahedral-like geometry (i) to avoid excited state distortions and (ii) to induce strong ligand field splitting, needed to shift the 4T_2 states toward higher energy thus preventing deactivation of the SF states due to back intersystem crossing (BISC).¹⁹ Complexes featuring SF states may be exploited as optical probes for oxygen²⁰, pressure²¹ and temperature,²² photocatalysis^{23–25} and photocathodic solar cells.^{19,26}

Concerning the luminescence activity associated with the SF transitions, the most promising results have been achieved so far by employing two families of Cr(III) complexes: $[Cr(ddpd)_2]^{3+}$ ($ddpd = N,N'$ -dimethyl- N,N'' -dipyridin-2-ylpyridine-2,6-diamine)^{18,27,28} and $[Cr(dqp)_2]^{3+}$ ($dqp = 2,6$ -di(quinolin-8-yl)pyridine).^{29,30} In those cases, the first coordination sphere is roughly octahedral, but the arrangement of the tridentate organic ligand around the Cr-center defines a λ/δ chirality in an overall D_2 geometry.³¹ Thanks to the electric dipole forbidden nature of the SF transition, in enantiopure form, such compounds display highly circularly polarized luminescence (CPL), with dissymmetry factors (g_{lum}) on the order of 10^{-1} .^{30–34} Such values are comparable with those obtained for the $f-f$ transitions of chiral lanthanide(III) complexes,^{35–39} but Cr offers the advantage of being cheaper, kinetically inert and more abundant than lanthanides.⁴⁰

^a Dipartimento di Chimica e Chimica Industriale, University of Pisa, via Moruzzi 13, 56124, Pisa, Italy

^b Department of Physics and Astronomy, University of Florence, via Sansone 1, 50019, Sesto Fiorentino, Italy

^c Department of Inorganic and Analytical Chemistry, University of Geneva, 30 quai E. Ansermet, CH-1211 Geneva 4, Switzerland

^d National High Magnetic Field Laboratory, Florida State University, Tallahassee, Florida 32310, USA

^e Departamento de Química Inorgánica, Facultad de Ciencias, University of Granada and "Unidad de Excelencia en Química (UEQ)", Avda. Fuente Nueva s/n, 18071, Granada, Spain.

E-mail:

jrijimenez@ugr.es, francesco.zinna@unipi.it

Electronic Supplementary Information (ESI) available: [details of any supplementary information available should be included here]. See DOI: 10.1039/x0xx00000x

ARTICLE

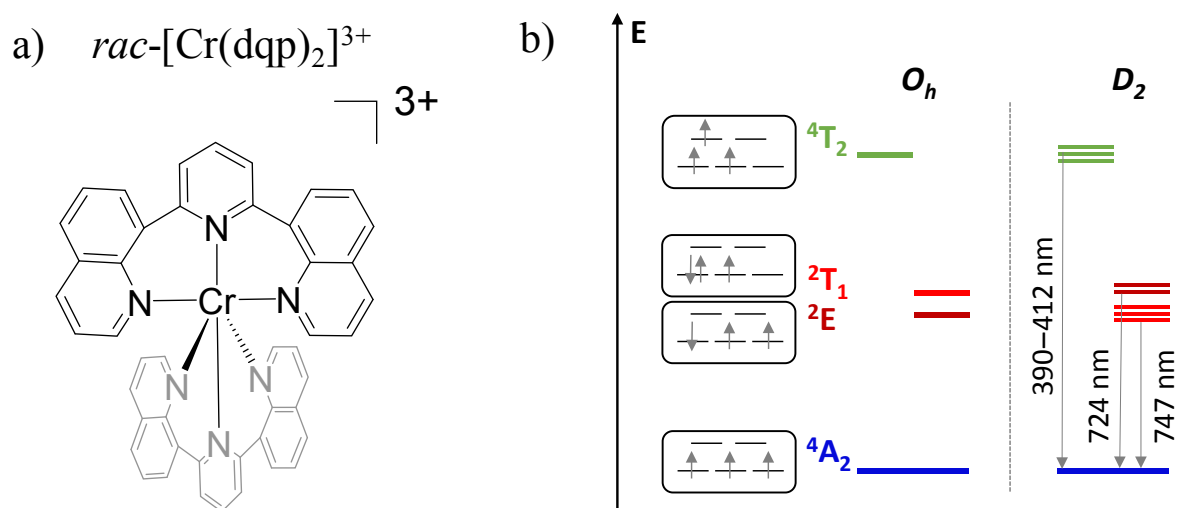


Figure 1. a. Structure of the complex. b. Electronic states of $[\text{Cr}(\text{dqp})_2]^{3+}$ in an ideal octahedral (O_h) and D_2 geometry; Note the ${}^2T_1/{}^2E$ level inversion from O_h to D_2 geometry.

A different technique to study the circular polarization of the emitted light is magnetic CPL (MCPL), where the physical origin of the CP emission is not the chirality of the material, but the effect is triggered by the application of an external magnetic field. This technique belongs to the family of magneto-optical spectroscopies, along with the more common Faraday rotation and magnetic circular dichroism (MCD).^{41–43} In a MCPL experiment, the circular polarization of the luminescence is studied, when the sample is placed under a magnetic field collinear with the emission direction, and excited with unpolarized light.^{44,45} Unlike CPL, MCPL may be displayed by both chiral and achiral luminescent systems and it does not depend on the enantiomer chirality. Indeed, CPL and MCPL follow very different selection rules. CPL is gauged by the scalar product $\mathbf{m}_{ng} \cdot \boldsymbol{\mu}_{gn}$, where \mathbf{m} and $\boldsymbol{\mu}$ are the magnetic and electric transition moments between the ground state g and excited state(s) n .⁴⁶ On the other hand, several mechanisms can lead to MCPL. Relatively strong signals are predicted in the case of orbital or spin degenerate ground or excited states, where the degeneracy is removed by the magnetic field due to the Zeeman effect. In these cases, the MCPL signal depends on $\mathbf{m}_{gg} \cdot \boldsymbol{\mu}_{ng} \boldsymbol{\mu}_{gn}$ and $\mathbf{m}_{nn} \cdot \boldsymbol{\mu}_{ng} \boldsymbol{\mu}_{gn}$ products (\mathbf{m}_{gg} and \mathbf{m}_{nn} are the static magnetic dipole moments of the ground and excited state), for a degenerate ground or excited state respectively.^{47,48} Those expressions are associated to the so-called Faraday A- and C-terms.^{44,47,49,50} Emitting compounds characterized by a strong spin-orbit coupling, which allows for a significant mixing of states, are good candidates for magnetooptical spectroscopies, including MCPL.

MCPL has been thus studied in the case of f - f transitions of lanthanide complexes,^{51–53} d -metals (such as Ru and Ir

complexes),^{54,55} organic and metallo-organics compounds.^{56–64} MCPL and MCD were also reported in early studies of Cr(III) inorganic structures.^{65,66} MCD was also used to study far red/near infrared (NIR) transitions in the case of Ir or Pt complexes,^{67,68} where their observation through emission, and thus MCPL, is challenging. On the other hand, emissive Cr(III) compounds are potentially a more suitable platform to address metal transitions through MCPL. On a fundamental level, an analysis of the MCPL spectrum can elucidate the nature of the excited and ground states, Zeeman effects, etc., and along with other techniques can help to understand the full picture of the photophysics of a complex system.⁴⁴ Moreover, MCPL-active compounds have recently found applications in OLEDs able to emit circularly polarized electroluminescence in a magnetic field (MCP-OLEDs),^{69–72} therefore there is also a practical interest in unveiling different types of emitters endowed with significant MCPL. In the following, we investigate the racemic $[\text{Cr}(\text{dqp})_2](\text{PF}_6)_3$ material by MCPL and MCD (Figure 1b). As introduced above, $[\text{Cr}(\text{dqp})_2]^{3+}$ is one of the archetypes of a molecular ruby and the same concept shown here may be applied to similar systems.

Results and Discussion

Optical and magneto-optical studies reported here were performed on deaerated acetonitrile solutions of the racemic compound $[\text{Cr}(\text{dqp})_2](\text{PF}_6)_3$. The photoluminescence (PL) spectrum of $[\text{Cr}(\text{dqp})_2]^{3+}$ shows two main emission bands centred at 750 and 729 nm (Figure 2), associated to the SF transitions (${}^2E/{}^2T_1 \rightarrow {}^4A_2$) from the sublevels of the doublet excited states (see Figure 1a) to the ground

state. The lower energy band appears more intense than the higher energy one by a factor of 1.53 at 300 K, due to a higher Boltzmann population with an energy gap of $\approx 420\text{ cm}^{-1}$ between the two bands.²⁷

We measured the MCPL emission at 300 K under a magnetic field of $\pm 0.4\text{ T}$ generated by a permanent magnet, exciting the sample at 365 nm (see the ESI and Figure S1 for the details of the measurement set-up). In these conditions, a relatively strong and slightly asymmetric bisignate MCPL band was observed corresponding to the higher energy doublet transition (Figure 2). Such band has a cross-over point at 725 nm, matching the maximum of the corresponding photoluminescence band. This derivative-like shape is consistent with a signal originating from Zeeman-split states (see below). The MCPL strength can be quantified by a magnetic field (H) normalized dissymmetry factor (g_{MCPL}), defined as:

$$g_{\text{MCPL}} = 2 \frac{I_L - I_R}{H(I_L + I_R)} \quad \text{Eq. 1}$$

where I_L and I_R are the left and right circularly polarized components of the emission under the magnetic field. In our case, we found a g_{MCPL} of $6.3 \cdot 10^{-3}\text{ T}^{-1}$ at 722 nm and $-2.1 \cdot 10^{-3}\text{ T}^{-1}$ at 733 nm. These values are in line with those obtained for other *d* or *f*-metal complexes.^{52–54,73} A much weaker ($\approx 0.9 \cdot 10^{-3}\text{ T}^{-1}$) band around 750 nm associated the lower energy SF transition was also observed. As expected, roughly mirror image MCPL spectra were obtained for \pm magnetic field (Figure S3a), by reversing the orientation of the permanent magnet. In Figure 2, we report the MCPL as the semi-difference of the polarized signal S obtained under positive ($S(+)$) and negative ($S(-)$) H, as:

$$\text{MCPL} = \frac{1}{2}[S(+)-S(-)] \quad \text{Eq. 2}$$

Positive and negative fields are here defined as parallel and anti-parallel to the *k*-vector, i.e. the propagating direction of light. Baseline effects and possible artefact signals due to photoselection cause some deviation from the mirror image relationship expected for spectra obtained under opposite magnetic field, especially in the case of small signals (Figure S3a). The data treated according to Eq. 2 ensures that such artefacts, which are magnetic field-independent, are eliminated and only the true MCPL is recovered (Figure S3b).

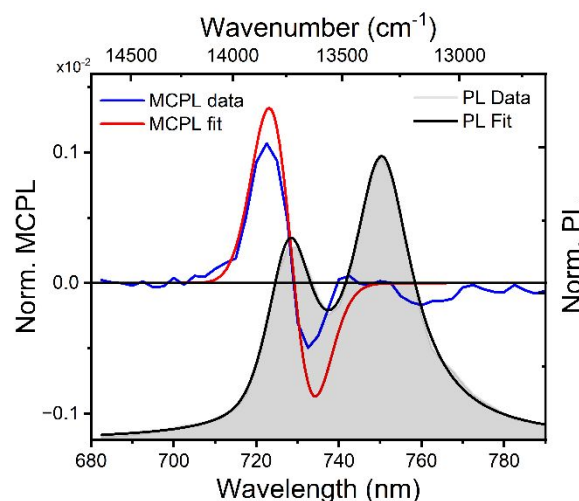


Figure 2. PL and MCPL at 0.4 T, normalized for the PL maximum, of the Cr^{3+} complex dissolved in deaerated acetonitrile, along with the corresponding fittings according to the rigid-shift model (see the text).

The same SF transitions were also studied in absorption through MCD, on a concentrated solution of the complex under $\pm 1.4\text{ T}$ magnetic field (Figure 3b), generated by an electromagnet. A derivative-like signal was observed associated to the higher energy doublet transition, similar to the corresponding MCPL band. No significant MCD corresponding to the lower energy SF transition was detected. Similarly to the MCPL, MCD dissymmetry factor (g_{MCD}) can be defined as:

$$g_{\text{MCD}} = 2 \frac{A_L - A_R}{H(A_L + A_R)} \quad \text{Eq. 3}$$

With A_L (A_R) the absorbance of left (right) circularly polarized light. The g_{abs} were estimated approximately $+1.7$ and $-1.4 \cdot 10^{-2}\text{ T}^{-1}$ at 725 and 728 nm respectively. Such values are 2 orders of magnitude higher than those observed for the MCD bands observed between 500 and 250 nm (Figure 3 a), associated with the ligand-centred (LC) and ligand-to-metal charge-transfer transitions ($g_{\text{MCD}} \approx 1 \cdot 10^{-4}\text{ T}^{-1}$). This confirms that magneto-optical techniques are excellent tools to study SF transitions. Such studies are particularly challenging in standard absorption spectroscopy experiments due to the very weak extinction coefficient of SF transitions (below $1\text{ M}^{-1}\text{ cm}^{-1}$, see Figure 3b), which requires high concentrations and deconvolution from the tail of the high energy absorption transitions, making it difficult to distinguish the extinction peaks from the instrumental noise. On the other hand, we show here that MCD experiments can give signals well above the instrumental noise, without the need for deconvolution procedures. As expected, the MCD signal intensity was found to be linear with the applied field H (Figure S4). The overall similarity of the MCD and MCPL shape and signature is consistent with minor structural differences between the ground state and the doublet states of Cr(III) . Indeed, SF states have a nested nature and therefore they are expected to be only weakly distorted with respect to the ground state.^{10,23}

To rationalize these results, it is worth analysing the states involved in the SF transitions giving origin to the MCD and MCPL spectra. In the complex, the presence of the helically twisted tridentate dq suppresses any symmetry plane and lowers the overall symmetry to D_2 . In such symmetry, the orbital degeneracy of the excited states is removed, and 2T_1 and 2E states are split into 3 and 2 components respectively (Figure 1a). The main MCPL signal at 729 nm is associated with the lower component of the doubly degenerate 2E state. A small contribution to the PL, giving non-significant MCPL, is observed at approximately 710 nm, possibly stemming from the higher energy component of the 2E state (Figure S2). Moreover, even in the absence of an external field, the orbitally-nondegenerate quartet ground state (4A_2) is split by the zero-field splitting (ZFS) into two Kramers doublets (KD) $| \pm 1/2 \rangle$ and $| \pm 3/2 \rangle$ (Figure 4).

To extract the ZFS and the corresponding spin Hamiltonian D and E parameters, we followed the method proposed by van Slageren *et*

al. (see ESI).⁷⁴ As the first step, the energies corresponding to the 3 ${}^4A_2 \rightarrow {}^4T_2$ term-to-term transitions were determined by a phenomenological deconvolution of the 360–500 nm region of the MCD spectrum (Figure S5). With this procedure, we identified the following energies, centred approximately at 24220, 24922 and 25630 cm^{-1} (Table S1). From these values (see ESI for the formulae in a D_2 geometry), we calculated D and E parameters as approximately 0.51 and 0.16 cm^{-1} , respectively, with a rhombicity factor $E/D=0.32$, close to the maximum (1/3). The corresponding ZFS was calculated to be $\approx 1.1 \text{ cm}^{-1}$ as $2\sqrt{D^2 + 3E^2}$ (see Figure 4). Despite the large error of the method (see for instance the standard errors on the fitting coefficient in Table S1), the values are comparable with those found for the analogue complex $[\text{Cr}(\text{ddpd})_2]^{3+}$,⁷⁴ and the values found by HFEPR (high-frequency and -field electron paramagnetic resonance) on our complex (see below).

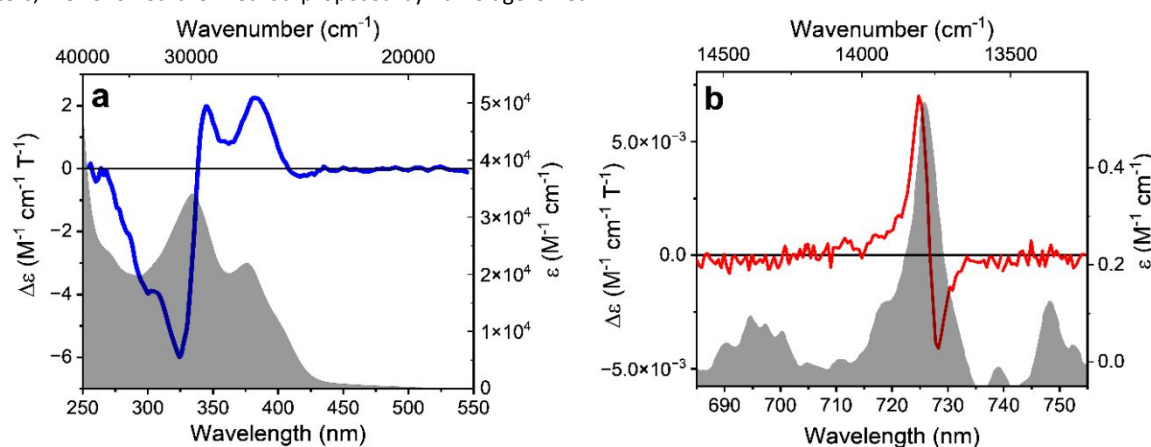


Figure 3. MCD and extinction spectra of an acetonitrile solution of $[\text{Cr}(\text{dqp})_2]^{3+}$, for the higher energy region (a) and for the SF transition region (b). The data are normalized for concentration, optical path and applied magnetic field.

We now focus our analysis on the MCPL and PL spectra at the NIR SF transitions. In the presence of an external magnetic field, the degeneracy of the KDs of the quartet ground states is removed by Zeeman effect giving 4 spin states: ideally $|+1/2\rangle$, $|-1/2\rangle$, $|+3/2\rangle$ and $|-3/2\rangle$. Similarly, the doublet excited states split into $|+1/2\rangle$ and $|-1/2\rangle$ states.

In the following, we focus only on the higher energy SF band around 729 nm, producing the main signal. In a reasonably simplified scheme, we consider only the transitions among Zeeman levels with $\Delta M_s = \pm 1$.⁷⁵ A $\Delta M_s > 0$ corresponds to a positive MCPL transition and vice versa, therefore a total of two closely spaced positive and two negative MCPL contributions are expected (Figure 4).

When the bands are separated by an energy much smaller than the bandwidth, the spectral features can be conveniently modelled by using the so-called rigid-shift approximation. This method is usually applied to model A- and C-Faraday terms in MCD.^{43,76,77} Within this model, PL and MCPL spectra are fitted simultaneously using a home-built MATLAB code, employing fitting functions that hold shared parameters. The emission is fitted with a bell-shaped function centred on the energy barycentre (unsplit levels), while the MCPL is

fitted with equal but opposite functions, displaced by the small field-induced splitting (see ESI and Figure S6). All the functions, used for both the PL and MCPL, share the same shape and bandwidth, and are therefore determined simultaneously in the fitting. To carry out this procedure, we used the four energy levels of the 4A_2 state determined by HFEPR at 0.4 T (see below), as fixed parameters. The fitting obtained through this model, by using pseudo-Voigt functions, closely retraces the experimental PL and MCPL data (Figure 2 and ESI). Similar results were obtained using purely Gaussian or Lorentzian functions, but pseudo-Voigt functions retrace better the PL and MCPL line shapes (Figure S7 and Table S2). The overestimation of the model with respect to the experimental MCPL data may be due to the fact that, in the case of ZFS with $E \neq 0$, the four states associated with 4A_2 cannot be described by a pure M_s quantum number as they are significantly mixed (see below). This would therefore impact the underlying assumption that each transition is completely circularly polarized. Notice that the lifetime of the excited state being sufficiently long ($\tau_{\text{obs}} = 1.2 \text{ ms}$),³³ the population of its Zeeman levels follows Boltzmann distribution. The Zeeman splitting being much smaller than room temperature thermal energy (207 cm^{-1} at 298 K), the Zeeman levels of the doublet excited states are almost

equally populated, as $1 - (\Delta E/k_b T) \approx 0.998$. Assuming the Zeeman splitting proportional to M_s ,⁷⁸ through the fitting, we found a field-normalized Zeeman splitting of $0.46 \text{ cm}^{-1} \text{ T}^{-1}$ and $1.38 \text{ cm}^{-1} \text{ T}^{-1}$ for the $|1/2\rangle$ and $|3/2\rangle$ states respectively. Figure 4 quantitatively summarizes the fine structure of the electronic level involved in the MCPL emission of the main band.

To corroborate the analysis and demonstrate the consistency of our approach, we performed magnetometry and EPR characterization. DC magnetometry, studied in the 2–300 K temperature range, confirms a quartet ground state (4A_2 , see supporting information and Figure S8). Saturation magnetization at 2 K is consistent with what expected for isolated Cr(III) cations with $g=2$ and $S=3/2$. Upon cooling, the $\chi_M T$ product remains almost constant until about 10 K and then sharply decreases to reach a value of $1.78 \text{ cm}^3 \text{ mol}^{-1} \text{ K}$ at 2 K. This decrease is due to the ZFS and Zeeman interactions. The simultaneous fitting of the susceptibility and magnetization data with the ZFS Hamiltonian using the PHI Software⁷⁹ leads to a $|D|$ value of 0.72 cm^{-1} , which is rather consistent with the values extracted from MCD and HFEPR spectroscopies.

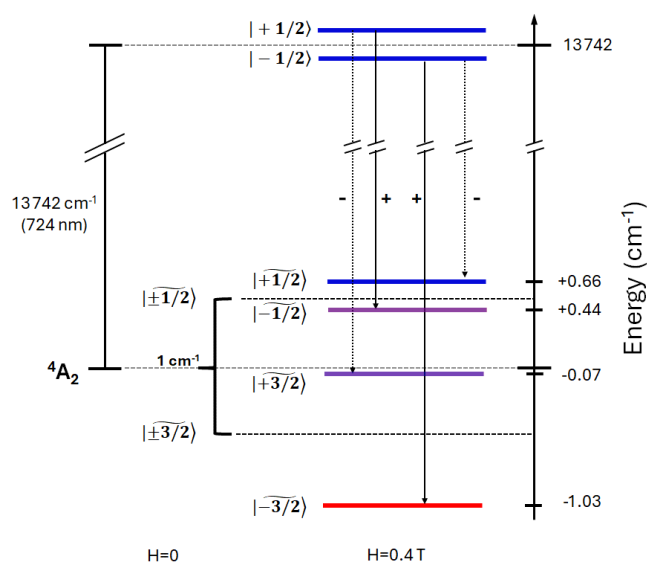


Figure 4. ZFS- and field-normalized Zeeman-split levels at 0.4 T corresponding to the main MCPL bands. The MCPL transitions are represented by the dotted arrows along with the expected sign. The + and – symbols indicate left and right circularly polarized emissive transitions respectively. The energies of ground state sublevels (for $B_0 \parallel z$) are obtained through HFEPR analysis (see Figure 5 and Table S3). As considerable mixing occurs (see Table S3), the predominant character of the M_s state is indicated by a \sim symbol. Purple colour indicates strongly mixed states.

To confirm the determined D and E values from MCD measurements, the Cr(III) compound was studied by HFEPR spectroscopy.⁸⁰ The shape and amplitude of the low-temperature (30 K) spectra of the powder sample “as is” (i.e. unconstrained) strongly suggested field-induced alignment (i.e. torquing) of the crystallites. Indeed, the resulting spectra could be very well simulated as originating from a

single crystal oriented with the z -axis of the ZFS tensor parallel to the magnetic field B_0 (Figure 5). At 270 GHz, the three dominating peaks between 8 and 12 T represent the allowed $\Delta M_s = \pm 1$ transitions between the spin sublevels of the $S = 3/2$ spin state of Cr(III). The weak peaks in the 3 – 6 T range are the nominally forbidden $\Delta M_s = \pm 2$ and ± 3 transitions. The structure visible on the peaks is an artefact that can be attributed to imperfect field alignment and is not simulated.

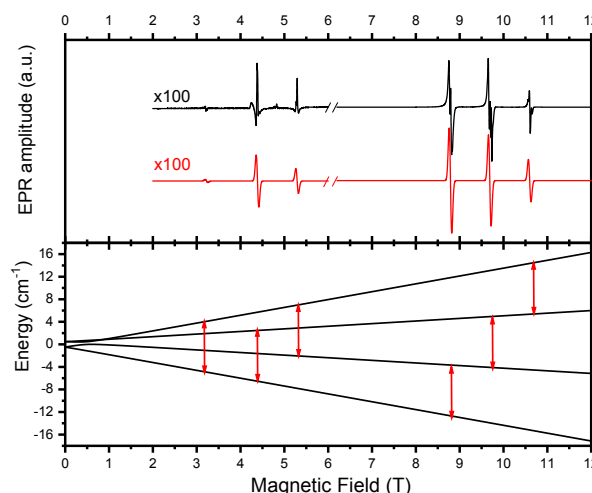


Figure 5. Top: EPR spectrum of a polycrystalline sample containing the Cr(III) compound at 30 K and 270 GHz (black trace) accompanied by its simulation (red trace) using the following spin Hamiltonian parameters: $S = 3/2$, $D = 0.42 \text{ cm}^{-1}$, $E = 0.14 \text{ cm}^{-1}$ ($E/D = 0.33$, maximum rhombicity limit), $g_{iso} = 1.99$. The simulation assumed a single crystal oriented with the z -axis of the ZFS tensor parallel to the magnetic field B_0 . Bottom: Representation of the energy levels for a $S = 3/2$ spin state at 270 GHz. The HFEPR transitions between the spin sublevels are marked with red arrows.

In order to extract the full set of frequency-independent spin Hamiltonian parameters, the sample was constrained using n -eicosane and pressed into a pellet (Figure S9). The resulting spectrum is accompanied by a simulation, this time assuming a powder distribution of the crystallites in space. The simulation parameters are modified relative to those used above to account for the slight asymmetry of the central line: $D = 0.43 \text{ cm}^{-1}$, $E = 0.14 \text{ cm}^{-1}$ ($E/D = 0.325$), $g_x = 1.99$, $g_{y,z} = 1.98$.

To finalize the values of frequency-independent spin Hamiltonian parameters, we built a two-dimensional map of turning points in pellet spectra and applied the tunable-frequency methodology⁸¹ by fitting the parameters simultaneously to that map. This resulted in the following values: $D = -0.436(7) \text{ cm}^{-1}$, $E = -0.144(7) \text{ cm}^{-1}$ ($E/D = 0.31$), $g_{iso} = 1.980(4)$ (Figure S10). The negative sign of D reproduced single-frequency spectra better than a positive value.

Altogether, these results are in good agreement with the ones that we found by MCPL and MCD experiments. Finally, the nature of the M_s states associated with 4A_2 was evaluated by calculating the mixing coefficients at 0.4 T (Table S3, S4, see also Figure S11 for an

expansion of HFEP levels at low field). The coefficients show (in the case of $B_0 \parallel z$, see Table S3) a strong mixing between two inner $|+3/2\rangle$ and $|-1/2\rangle$ levels, responsible for the avoided level crossing near 1 T visible in Figure 5 (bottom), while the outer levels retain mostly their $|+1/2\rangle$ and $|-3/2\rangle$ character.

Conclusions

Beyond the many areas of interest in Cr(III) SF transitions of the molecular ruby $[\text{Cr}(\text{dqp})_2]^{3+}$, we show here that they also display a strong MCPL activity. MCD and MCPL techniques are here applied to elucidate the fine structure of the levels involved in the SF transitions. In particular, the analysis of SF transition through MCPL was consistent with the energies found with the more established EPR spectroscopy. Such possibilities offered by magneto-optical techniques can be exploited to gather more insight into the photophysics of SF transitions in related cases, e.g. in view of optical read-out of molecular qubits. Moreover, it opens up new opportunities such as applications in magneto-optical and magnetoelectronic devices.

Author Contributions

Conceptualization: F.Z.; Data curation: A.G., G.P., F.P., J.R.J., F.Z.; Formal Analysis: A.G., F.Z.; Resources: M.P., C.P., J.R.J.; Funding acquisition: L.D.B., C.P., F.P., J.R.J.; Investigation: A.G., L.C., E.C., J.K., F.Z. Methodology: F.Z., G.P. Writing – original draft: A.G., J.R.J., F.Z.; Writing – review & editing: all authors.

Conflicts of interest

There are no conflicts to declare.

Acknowledgements

We would like to thank Mr David Michelotti for technical support with the MCPL set-up. F.P. acknowledges MUR through PRIN-PNRR project (P20229723Z) J.R.J. thanks Ministerio de Ciencia Innovación y Universidades for a Ramón y Cajal contract (grant RYC2022-037255-I) funded by MCIN/AEI/10.13039/501100011033 and FSE+. Part of this work was funded by the National High Magnetic Field Laboratory which is funded by the US National Science Foundation (Cooperative Agreement DMR-212856) and the State of Florida. Dr. A. Ozarowski (NHMFL) is acknowledged for his EPR fit and simulation software SPIN and help with solving the level mixing problem. Prof. L. Sorace (University of Florence) is acknowledged for fruitful discussions.

Notes and references

- V. Balzani, A. Credi and M. Venturi, *Coord. Chem. Rev.*, 1998, **171**, 3–16.
- J. Twilton, C. (Chip) Le, P. Zhang, M. H. Shaw, R. W. Evans and D. W. C. MacMillan, *Nat Rev Chem*, 2017, **1**, 1–19.
- H. Xu, R. Chen, Q. Sun, W. Lai, Q. Su, W. Huang and X. Liu, *Chem. Soc. Rev.*, 2014, **43**, 3259–3302.
- W. C. H. Choy, W. K. Chan and Y. Yuan, *Adv. Mater.*, 2014, **26**, 5368–5399.
- M. P. Coogan and V. Fernández-Moreira, *Chem. Commun.*, 2013, **50**, 384–399.
- J. Berrones Reyes, M. K. Kuimova and R. Vilar, *Curr. Opin. Chem. Biol.*, 2021, **61**, 179–190.
- Y. Wu, S. Li, Y. Chen, W. He and Z. Guo, *Chem. Sci.*, 2022, **13**, 5085–5106.
- T. W. Rees, P.-Y. Ho and J. Hess, *ChemBioChem*, 2023, **24**, e202200796.
- C. B. Smith, L. C. Days, D. R. Alajroush, K. Faye, Y. Khodour, S. J. Beebe and A. A. Holder, *Photochem. Photobiol.*, 2022, **98**, 17–41.
- W. R. Kitzmann, J. Moll and K. Heinze, *Photochem Photobiol Sci*, 2022, **21**, 1309–1331.
- M. Dorn, J. Kalmbach, P. Boden, A. Kruse, C. Dab, C. Reber, G. Niedner-Schatteburg, S. Lochbrunner, M. Gerhards, M. Seitz and K. Heinze, *Chem. Sci.*, 2021, **12**, 10780–10790.
- M. Dorn, D. Hunger, C. Förster, R. Naumann, J. van Slageren and K. Heinze, *Chem. Eur. J.*, 2023, **29**, e202202898.
- M. Dorn, J. Kalmbach, P. Boden, A. Pöpcke, S. Gómez, C. Förster, F. Kuczelinis, L. M. Carrella, L. A. Büldt, N. H. Bings, E. Rentschler, S. Lochbrunner, L. González, M. Gerhards, M. Seitz and K. Heinze, *J. Am. Chem. Soc.*, 2020, **142**, 7947–7955.
- J. P. Harris, C. Reber, H. E. Colmer, T. A. Jackson, A. P. Forshaw, J. M. Smith, R. A. Kinney and J. Telsner, *Can. J. Chem.*, 2017, **95**, 547–552.
- N. R. East, R. Naumann, C. Förster, C. Ramanam, G. Diezemann and K. Heinze, *Nat. Chem.*, 2024, 1–8.
- W. R. Kitzmann, D. Hunger, A.-P. M. Reponen, C. Förster, R. Schoch, M. Bauer, S. Feldmann, J. van Slageren and K. Heinze, *Inorg. Chem.*, 2023, **62**, 15797–15808.
- Q. Yao and A. W. Maverick, *Inorg. Chem.*, 1988, **27**, 1669–1670.
- C. Wang, S. Otto, M. Dorn, E. Kreidt, J. Lebon, L. Sršan, P. Di Martino-Fumo, M. Gerhards, U. Resch-Genger, M. Seitz and K. Heinze, *Angew. Chem. Int. Ed.*, 2018, **57**, 1112–1116.
- S. Treiling, C. Wang, C. Förster, F. Reichenauer, J. Kalmbach, P. Boden, J. P. Harris, L. M. Carrella, E. Rentschler, U. Resch-Genger, C. Reber, M. Seitz, M. Gerhards and K. Heinze, *Angew. Chem. Int. Ed.*, 2019, **58**, 18075–18085.
- C. Wang, S. Otto, M. Dorn, K. Heinze and U. Resch-Genger, *Anal. Chem.*, 2019, **91**, 2337–2344.
- S. Otto, J. P. Harris, K. Heinze and C. Reber, *Angew. Chem. Int. Ed.*, 2018, **57**, 11069–11073.
- S. Otto, N. Scholz, T. Behnke, U. Resch-Genger and K. Heinze, *Chem. Eur. J.*, 2017, **23**, 12131–12135.
- W. R. Kitzmann and K. Heinze, *Angew. Chem. Int. Ed.*, 2023, **62**, e202213207.
- T. H. Bürgin, F. Glaser and O. S. Wenger, *J. Am. Chem. Soc.*, 2022, **144**, 14181–14194.
- C. Wang, H. Li, T. H. Bürgin and O. S. Wenger, *Nat. Chem.*, 2024, 1–9.
- B. Doistau, G. Collet, E. A. Bolomey, V. Sadat-Noorbakhsh, C. Besnard and C. Piguet, *Inorg. Chem.*, 2018, **57**, 14362–14373.
- S. Otto, M. Grabolle, C. Förster, C. Kreitner, U. Resch-Genger and K. Heinze, *Angew. Chem. Int. Ed.*, 2015, **54**, 11572–11576.
- S. Otto, C. Förster, C. Wang, U. Resch-Genger and K. Heinze, *Chem. Eur. J.*, 2018, **24**, 12555–12563.
- J.-R. Jiménez, M. Poncet, B. Doistau, C. Besnard and C. Piguet, *Dalton Trans.*, 2020, **49**, 13528–13532.

- 30 J.-R. Jiménez, B. Doistau, C. M. Cruz, C. Besnard, J. M. Cuerva, A. G. Campaña and C. Piguet, *J. Am. Chem. Soc.*, 2019, **141**, 13244–13252.
- 31 M. Poncet, A. Benchohra, J.-R. Jiménez and C. Piguet, *ChemPhotoChem*, 2021, **5**, 880–892.
- 32 C. Dee, F. Zinna, W. R. Kitzmann, G. Pescitelli, K. Heinze, L. D. Bari and M. Seitz, *Chem. Commun.*, 2019, **55**, 13078–13081.
- 33 J.-R. Jiménez, M. Poncet, S. Míguez-Lago, S. Grass, J. Lacour, C. Besnard, J. M. Cuerva, A. G. Campaña and C. Piguet, *Angew. Chem. Int. Ed.*, 2021, **60**, 10095–10102.
- 34 J.-R. Jiménez, S. Míguez-Lago, M. Poncet, Y. Ye, C. L. Ruiz, C. M. Cruz, A. G. Campaña, E. Colacio, C. Piguet and J. M. Herrera, *J. Mater. Chem. C*, 2023, **11**, 2582–2590.
- 35 O. G. Willis, F. Zinna and L. Di Bari, *Angew. Chem. Int. Ed.*, 2023, **62**, e202302358.
- 36 L. Llanos, P. Cancino, P. Mella, P. Fuentealba and D. Aravena, *Coord. Chem. Rev.*, 2024, **505**, 215675.
- 37 H.-Y. Wong, W.-S. Lo, K.-H. Yim and G.-L. Law, *Chem*, 2019, **5**, 3058–3095.
- 38 F. Zinna and L. Di Bari, *Chirality*, 2015, **27**, 1–13.
- 39 B. Doistau, J.-R. Jiménez and C. Piguet, *Front. Chem.*, , DOI:10.3389/fchem.2020.00555.
- 40 C. Förster and K. Heinze, *Chem. Soc. Rev.*, 2020, **49**, 1057–1070.
- 41 P. N. Schatz, A. J. McCaffery, W. Suetaka, G. N. Henning, A. B. Ritchie and P. J. Stephens, *J. Chem. Phys.*, 1966, **45**, 722–734.
- 42 P. J. Stephens, W. Suëtaak and P. N. Schatz, *J. Chem. Phys.*, 1966, **44**, 4592–4602.
- 43 W. R. Mason, *A practical guide to magnetic circular dichroism spectroscopy*, Wiley-Interscience, Hoboken, N.J., 2007.
- 44 F. Zinna and G. Pescitelli, *Eur. J. Org. Chem.*, 2023, **26**, e202300509.
- 45 M. Fusè, G. Mazzeo, S. Ghidinelli, A. Evidente, S. Abbate and G. Longhi, *Spectrochim. Acta A*, 2024, **319**, 124583.
- 46 J. P. Riehl and F. S. Richardson, *Chem. Rev.*, 1986, **86**, 1–16.
- 47 J. P. Riehl and F. S. Richardson, *J. Chem. Phys.*, 1977, **66**, 1988–1998.
- 48 L. D. Barron, *Molecular Light Scattering and Optical Activity*, Cambridge University Press, 2009.
- 49 P. J. Stephens, *J. Chem. Phys.*, 1970, **52**, 3489–3516.
- 50 Z. Nelson, L. Delage-Laurin and T. M. Swager, *J. Am. Chem. Soc.*, 2022, **144**, 11912–11926.
- 51 F. S. Richardson and H. G. Brittain, *J. Am. Chem. Soc.*, 1981, **103**, 18–24.
- 52 T. Wu, J. Kapitán, V. Andrushchenko and P. Bouř, *Anal. Chem.*, 2017, **89**, 5043–5049.
- 53 H. Yoshikawa, G. Nakajima, Y. Mimura, T. Kimoto, Y. Kondo, S. Suzuki, M. Fujiki and Y. Imai, *Dalton Trans.*, 2020, **49**, 9588–9594.
- 54 M. Kitahara, S. Suzuki, K. Matsudaira, S. Yagi, M. Fujiki and Y. Imai, *ChemistrySelect*, 2021, **6**, 11182–11187.
- 55 E. Krausz, G. Moran and H. Riesen, *Chem. Phys. Lett.*, 1990, **165**, 401–406.
- 56 S. Jena, S. K. Behera, J. Eyyathiyil, M. Kitahara, Y. Imai and P. Thilagar, *Adv. Opt. Mater.*, 2023, **11**, 2300923.
- 57 S. Ghidinelli, S. Abbate, G. Mazzeo, L. Paoloni, E. Viola, C. Ercolani, M. P. Donzello and G. Longhi, *Chirality*, 2020, **32**, 808–816.
- 58 S. Ghidinelli, S. Abbate, G. Mazzeo, R. Paolesse, G. Pomarico and G. Longhi, *ACS Omega*, 2021, **6**, 26659–26671.
- 59 Q. Jin, S. Chen, Y. Sang, H. Guo, S. Dong, J. Han, W. Chen, X. Yang, F. Li and P. Duan, *Chem. Commun.*, 2019, **55**, 6583–6586.
- 60 H. Toda, N. Hara, M. Fujiki and Y. Imai, *RSC Adv.*, 2021, **11**, 1581–1585.
- 61 H. Toda, S. Otake, A. Ito, M. Miyasaka, M. Fujiki and Y. Imai, *ChemPhysChem*, 2021, **22**, 2058–2062.
- 62 N. Hara, M. Kitahara, T. Sugimura, H. Toda, M. Shizuma, A. Ito, M. Miyasaka, M. Fujiki and Y. Imai, *Phys. Chem. Chem. Phys.*, 2021, **23**, 8236–8240.
- 63 R. Amasaki, M. Kitahara, T. Kimoto, M. Fujiki and Y. Imai, *Eur. J. Inorg. Chem.*, 2022, **2022**, e202101066.
- 64 T. Tomikawa, Y. Kitagawa, K. Yoshioka, K. Murata, T. Miyatake, Y. Hasegawa and K. Ishii, *J. Mater. Chem. C*, 2023, **11**, 2831–2835.
- 65 R. A. Shatwell and A. J. McCaffery, *Mol. Phys.*, 1975, **30**, 1489–1504.
- 66 A. J. McCaffery, P. Brint, R. Gale and R. A. Shatwell, *Chem. Phys. Lett.*, 1973, **22**, 600–602.
- 67 K. Murata and K. Ishii, *European Journal of Inorganic Chemistry*, 2017, **2017**, 5103–5107.
- 68 K. Ishii, J. Wada and K. Murata, *J. Phys. Chem. Lett.*, 2020, **11**, 9828–9833.
- 69 K. Hara, A. Morimoto, K. Matsudaira, S. Suzuki, S. Yagi, M. Fujiki and Y. Imai, *ChemPhotoChem*, 2022, **6**, e202100253.
- 70 T. Kuroda, M. Kitahara, S. Yagi and Y. Imai, *Front. Chem.*, , DOI:10.3389/fchem.2023.1281168.
- 71 M. Kitahara, K. Hara, S. Suzuki, H. Iwasaki, S. Yagi and Y. Imai, *Organic Electronics*, 2023, **119**, 106814.
- 72 S. Suzuki, Y. Yamamoto, M. Kitahara, R. Shikura, S. Yagi and Y. Imai, *J. Mater. Chem. C*, 2024, **12**, 3430–3436.
- 73 Y. Imai, *ChemPhotoChem*, 2021, **5**, 969–973.
- 74 S. Lenz, H. Bamberger, P. P. Hallmen, Y. Thiebes, S. Otto, K. Heinze and J. van Slageren, *Phys. Chem. Chem. Phys.*, 2019, **21**, 6976–6983.
- 75 E. I. Solomon, M. L. Neidig and G. Schenk, in *Comprehensive Coordination Chemistry II*, Elsevier, 2003, pp. 339–349.
- 76 A. Gabbani, G. Petrucci and F. Pineider, *J. Appl. Phys.*, 2021, **129**, 211101.
- 77 A. Gabbani, G. Campo, V. Bonanni, P. van Rhee, G. Bottaro, C. de Julián Fernández, V. Bello, E. Fantechi, F. Biccari, M. Gurioli, L. Armelao, C. Sangregorio, G. Mattei, P. Christianen and F. Pineider, *J. Phys. Chem. C*, 2022, **126**, 1939–1945.
- 78 A. Kamińska, A. Suchocki, S. Kobayakov, L. Arizmendi, M. Potemski and F. J. Teran, *Phys. Rev. B*, 2007, **76**, 144117.
- 79 N. F. Chilton, R. P. Anderson, L. D. Turner, A. Soncini and K. S. Murray, *J. Comput. Chem.*, 2013, **34**, 1164–1175.
- 80 J. Krzystek, A. Ozarowski and J. Telser, *Coord. Chem. Rev.*, 2006, **250**, 2308–2324.
- 81 J. Krzystek, S. A. Zvyagin, A. Ozarowski, S. Trofimenko and J. Telser, *J. Magn. Reson.*, 2006, **178**, 174–183.

Supporting information

Magnetic circularly polarized luminescence from spin flip transitions in a molecular ruby

Alessio Gabbani,^{a,b} Maxime Poncet,^c Gennaro Pescitelli,^a Laura Carbonaro,^a **J.** Krzystek,^d Enrique Colacio,^e Claude Piguet,^c Francesco Pineider,^{a,b} Lorenzo Di Bari,^a Juan-Ramón Jiménez*,^e Francesco Zinna*^a

^a Dipartimento di Chimica e Chimica Industriale, University of Pisa, via Moruzzi 13, 56124, Pisa, Italy

^b Department of Physics and Astronomy, University of Florence, via Sansone 1, 50019, Sesto Fiorentino, Italy

^c Department of Inorganic and Analytical Chemistry, University of Geneva, 30 quai E. Ansermet, CH-1211 Geneva 4, Switzerland

^d National High Magnetic Field Laboratory, Florida State University, Tallahassee, Florida 32310, USA

^e Departamento de Química Inorgánica, Facultad de Ciencias, Universidad de Granada and Unidad de Excelencia en Química (UEQ), Avda. Fuente Nueva s/n, 18071, Granada, Spain.

E-mail:

jrjimenez@ugr.es, francesco.zinna@unipi.it

Complex Preparation

The $[\text{Cr}(\text{dqp})_2](\text{PF}_6)_3$ (dqp = 2,6-di(quinolin-8-yl)pyridine) has been prepared according to a published method.¹

Instrumentation

MCD measurements were carried out using an in-house built, lab-scale instrument equipped with a 1.4 T electromagnet. Light emitted by a 300 W Xe arc lamp (Newport) is monochromated (Newport Oriel Cornerstone 260) and chopped at 440 Hz. Polarization modulation at 47 kHz between LCP and RCP is obtained with a Glan-Thompson polarizer coupled to a photoelastic modulator (Hinds Instruments PEM 100) set to $\lambda/4$ retardation. The beam is then directed through the bore of an electromagnet (Buckley Systems Ltd. GMW model 3470) where the sample is placed. Light is collected by a photomultiplier tube (Hamamatsu R376). After transimpedance amplification, the output voltage of the detector is fed to two lock-in amplifiers, one referenced to the polarization modulation frequency (Stanford Research Systems SR850) and one to the light chopping frequency (Signal Recovery 7280); the ratio of the two signals is taken as the differential absorption (dichroism) ΔA . MCD signal is then obtained by the semi difference between the signals obtained at +1.4 T and -1.4 T. Calibration of the MCD signal is carried out against an aqueous solution of $[\text{Fe}(\text{CN})_6]^{3+}$ of known concentration. The MCD spectra of the Cr^{3+} complex were recorded in CH_3CN solution in a 1 mm optical path cuvette. The concentration was $1.67 \cdot 10^{-4}$ M and $2.57 \cdot 10^{-2}$ M for the high and low energy region respectively. Given the slits used (0.6 mm) and the grating employed in the monochromator, the spectral resolution was 1.9 nm. MCD vs field plots in the +1.4/-1.4 T range were also acquired by regulating the current passing in the coils of the electromagnet. The strength of the magnetic field was measured with a Hall probe.

MCPL measurements were carried out with an in-house built set-up mounted on an open optical bench (Figure S1). The sample is placed in front of 0.4 T NdFeB permanent magnet, and it is excited with a 365 nm LED (M365D1, Thorlabs) with a 0° geometry, using a dichroic mirror (cutoff 400 nm). The collected light is passed through a photoelastic modulator (Hinds Instruments PEM 100) set to $\lambda/4$ retardation modulated at 50 kHz, coupled with a Glan-Thompson polarizer. Ambient light is filtered out using a chopper. The light emitted by the sample then passes through a monochromator (Oriel Cornerstone 130) and is detected by a mutlialkali photomultiplier tube (Hamamatsu R376). The monochromator slits were set to 0.7 mm (spectral resolution of 9 nm), as this was found to be a good compromise between having enough light at the detector while ensuring enough spectral resolution to distinguish the two SF transitions (Figure S1). The voltage of the photomultiplier tube used was 650 V. After transimpedance amplification, the output voltage of the detector is fed to two lock-in amplifiers, one referenced to the polarization modulation frequency (MFLI, Zurich Instruments) and one to the light chopping frequency (Stanford Research Systems SR850). The PL and MCPL spectra are acquired simultaneously by using a LabVIEW routine. The spectra were recorded in a 2 mM CH_3CN solution, in Ar atmosphere, using a rotaflow 1 mm cuvette and deaerated CH_3CN as solvent. 9 spectra for each field (+0.4 and -0.4 T) were acquired and averaged. The excitation LED was powered with a current of 250 mA. The resulting excitation optical power was 48 mW, as measured with a power meter.

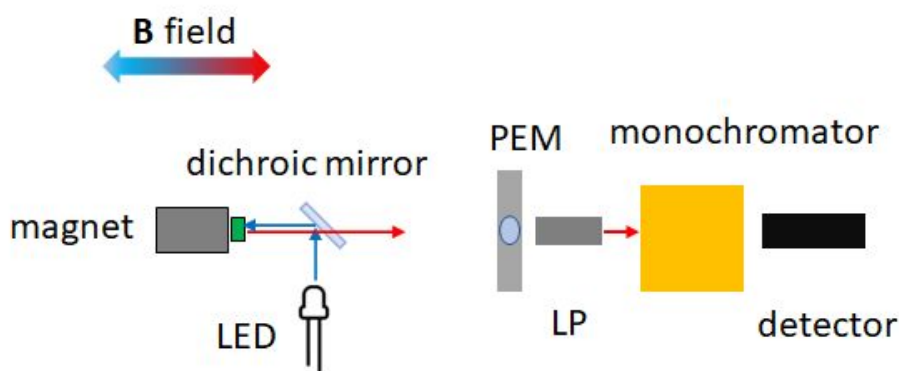


Figure S1. Simplified scheme of the set up employed for MCPL measurements.

High-frequency and -field EPR (HFEPR) spectra were recorded at the National High Magnetic Field Laboratory on 49 mg of polycrystalline sample either loose (unconstrained) or pressed into a pellet with *n*-eicosane. A homodyne spectrometer at the EMR Facility associated with a 15/17-T superconducting magnet is described in bibliography² with a modification of using a Virginia Diodes (VDI, Charlottesville, VA, USA) chain operating in the 48 – 540 GHz frequency range. Detection was provided with an InSb hot electron bolometer (QMC Ltd., Cardiff, UK). The magnetic field was modulated at 50 kHz for detection purposes. A Stanford Research Systems SR830 lock-in amplifier converted the modulated signal to *dc* voltage.

Variable-temperature (2–300 K) magnetic susceptibility measurements were carried out on polycrystalline samples under an applied field of 0.3 T using a DynaCool PPMS-9 physical measurement equipment. The magnetic susceptibility values were corrected from the diamagnetism of the molecular constituents and of the sample holder.

Additional figures

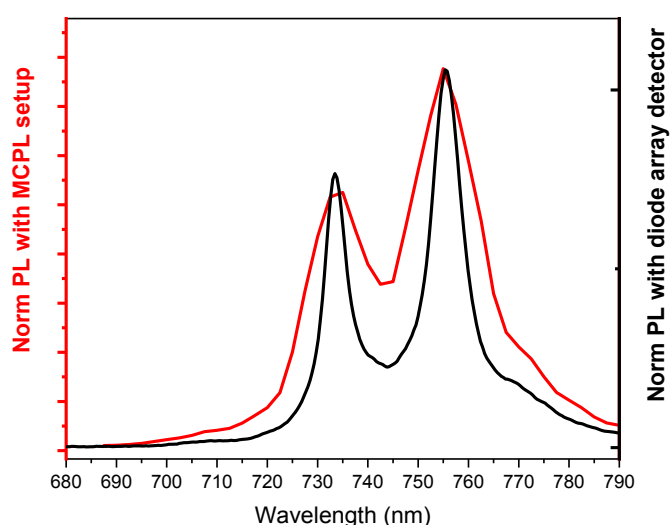


Figure S2: Comparison between the PL measured with the MCPL setup with a spectral resolution of 9 nm, and the one measured with an array detector having 2 nm of spectral resolution (Optosky ATP2000P Modular spectrometer, Crisel Instruments).

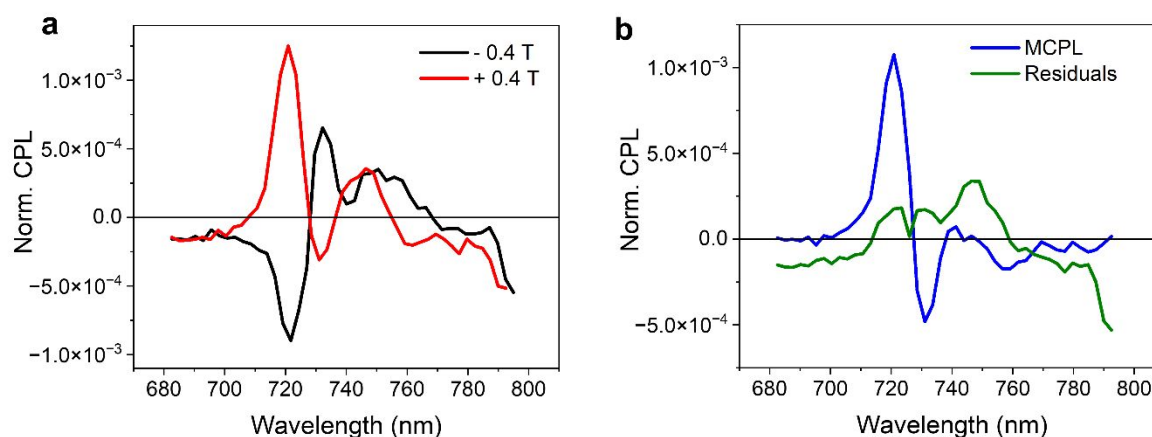


Figure S3. a. Normalized MCPL signals under ± 0.4 T; b. MCPL spectrum obtained by the semi-difference of the signals in a (see eq. 2 in the text), and the residuals obtained as the semi-sum of the signals.

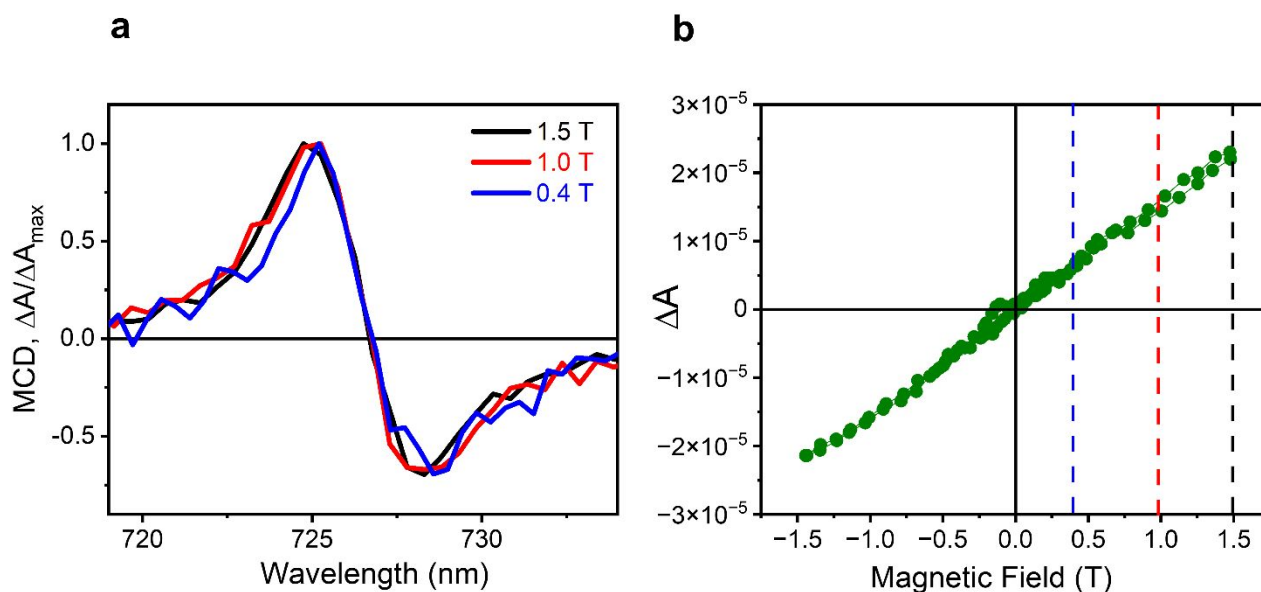


Figure S4. a. MCD spectrum of the most intense the spin-flip transition at different applied magnetic fields; b. MCD signal at 725 nm as a function of the applied magnetic field. The vertical lines in b show the applied field used to acquire the spectra in a.

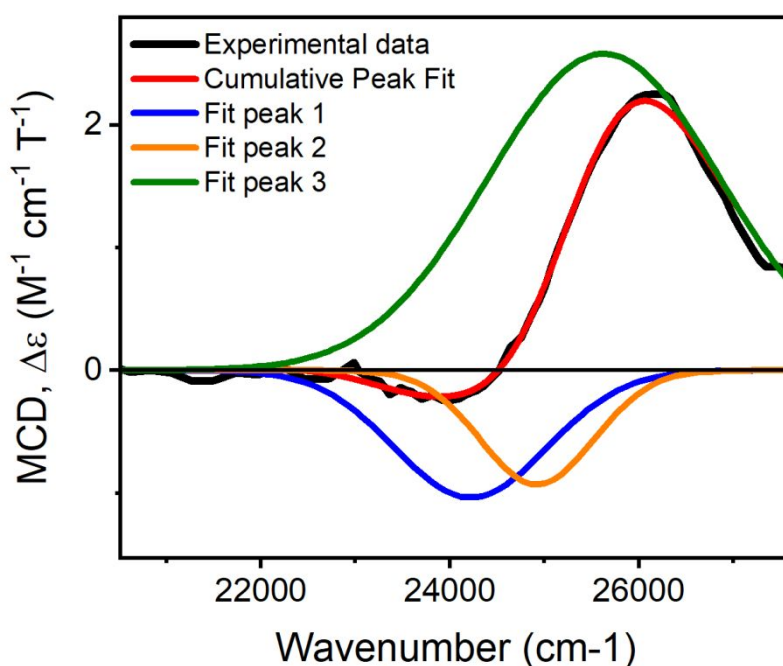


Figure S5. Phenomenological fitting of the low energy tail of the MCD spectrum.

Table S1. Values obtained from the fitting of the low energy tail of the MCD spectrum.

	Parameter ^a	Value	Standard Error
Peak 1	E	24220 cm ⁻¹	3112 cm ⁻¹
	A	-838	13
	σ	809 cm ⁻¹	1186 cm ⁻¹
Peak 2	E	24922 cm ⁻¹	356 cm ⁻¹
	A	-559	15
	σ	601 cm ⁻¹	394 cm ⁻¹
Peak 3	E	25630 cm ⁻¹	795 cm ⁻¹
	A	3175	19
	σ	1228 cm ⁻¹	271 cm ⁻¹

^a E = energy, A = area of the Gaussian, σ = peak full width at half maximum.

According to Lenz *et al.*³, in a D_2 geometry, the zero-field parameters D and E can be calculated taking into account the energies ΔE_i of the 3 components of the $^4A_2 \rightarrow ^4T_2$ transitions (with $\Delta E_3 > \Delta E_2 > \Delta E_1$):

$$D = \frac{1}{2}\zeta^2 \left(\frac{8}{\Delta E_1} - \frac{4}{\Delta E_2} - \frac{4}{\Delta E_3} \right) \quad (\text{eq S1})$$

$$E = \frac{1}{2}\zeta^2 \left(\frac{4}{\Delta E_2} - \frac{4}{\Delta E_3} \right) \quad (\text{eq S2})$$

Where ζ is spin-orbit coupling constant of the free Cr(III) ion (273 cm⁻¹).⁴ The ZFS can be calculated as:

$$\text{ZFS} = 2\sqrt{D^2 + 3E^2} \quad (\text{eq S3})$$

Analysis of MCPL data

According to the rigid shift model, the MCPL can be modelled by two equal, but opposite, bell-shaped functions displaced by the Zeeman splitting (Z), with respect to the barycenter energy (E). Such functions share the same parameters with the one used to fit the photoluminescence band (with the same bandwidth σ , peak area, etc.) and are obtained by simultaneously fitting the MCPL and the PL (Figure S6).

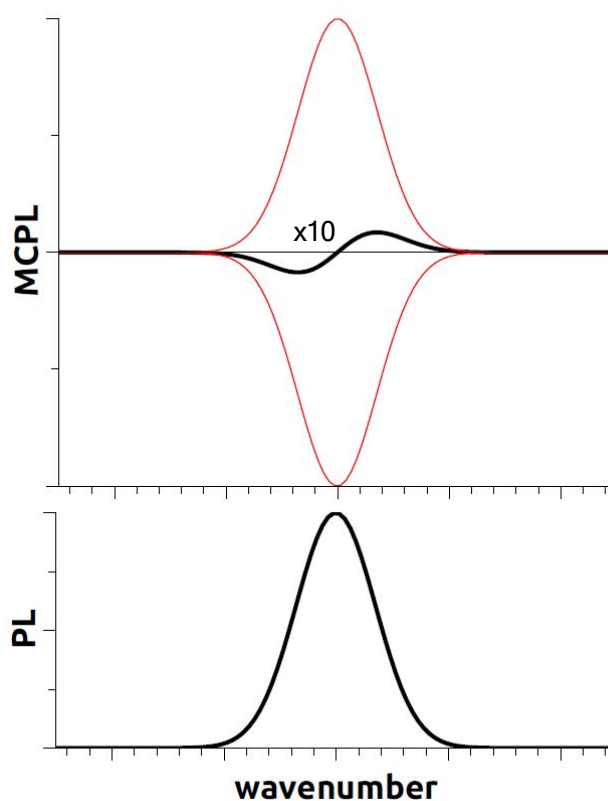


Figure S6. Illustrative example of the rigid-shift approximation applied to MCPL. The derivative shape (amplified 10 times for the sake of visualization) emerges from the partial cancellation of two opposite sign identical Gaussian functions translated by a dx (here $\sigma/dx = 100$)

Fitting functions

We chose pseudo-Voigt line shapes (eq S12) to fit the PL spectra, one for each of the two emissive transitions.

$$PL_i = A_i \left[\mu_i \frac{2}{\pi} \frac{\sigma_i}{4(x-E_i)^2 + \sigma_i^2} + (1 - \mu_i) \frac{\sqrt{4\log 2}}{\sqrt{\pi}\sigma_i} \exp\left(\frac{-4\log 2 \cdot (x-E_i)^2}{\sigma_i^2}\right) \right] \quad (\text{eq S4})$$

With $i = 1, 2$, where A_i is the peak Area, σ_i the full width at half maximum, E_i is the energy centre of the PL peak, while μ_i is a shape parameter with values in the range from 0 to 1, with 1 representing a pure Lorentzian shape and 0 a pure Gaussian shape.

MCPL of each SF transition is modelled as the difference between two sets of peak functions (two positive and two negative) with the same parameters used in equation S12 to fit the PL spectrum, but shifted in energy by a factor ΔE_i . Each fitting function used to model MCPL is therefore:

$$MCPL_i = \pm \frac{1}{2}(A_i \pm dA_i) \left[\mu_i \frac{2}{\pi} \frac{\sigma_i}{4(x-E_i-\Delta E_i)^2 + \sigma_i^2} + (1 - \mu_i) \frac{\sqrt{4\log 2}}{\sqrt{\pi}\sigma_i} \exp\left(\frac{-4\log 2 \cdot (x-E_i-\Delta E_i)^2}{\sigma_i^2}\right) \right] \quad (\text{eq S5})$$

where dA_i is added as an empirical parameter accounting for the slight asymmetry of the MCPL derivative-like signal. ΔE_i is expressed using the energy of the ground state sublevels found through HFEPR analysis. In particular, for the 4 transitions depicted in Figure 4 (main text), ΔE_i is reduced to the following expressions for $i = 1 - 4$:

$$|+1/2\rangle \rightarrow |-1/2\rangle : \quad \Delta E_1 = +\frac{Z}{2} - 0.44 \text{ cm}^{-1} \quad (\text{eq S6})$$

$$|-1/2\rangle \rightarrow |-3/2\rangle : \quad \Delta E_2 = -\frac{Z}{2} + 1.03 \text{ cm}^{-1} \quad (\text{eq S7})$$

$$|-1/2\rangle \rightarrow |+1/2\rangle : \quad \Delta E_3 = -\frac{Z}{2} - 0.66 \text{ cm}^{-1} \quad (\text{eq S8})$$

$$|+1/2\rangle \rightarrow |+3/2\rangle : \quad \Delta E_4 = +\frac{Z}{2} + 0.07 \text{ cm}^{-1} \quad (\text{eq S9}),$$

Where Z is considered as: $Z = \mu_B g H \Delta M_s = 0.36 \text{ cm}^{-1}$ (μ_B is the Bohr magneton and g the electron g -factor), for 0.4 T of applied field and $\Delta M_s = 1$, and is thus kept as a fixed parameter during the fitting. Note that the transitions associated to the energies in eq. give a positive sign contribution to MCPL, while those associated to eq. give a negative contribution (compare with Figure 4).

As it is very weak, in first approximation we neglect the low energy transition in the MCPL fitting functions.

Thus, equations S4 and S5 are used to fit simultaneously the PL and MCPL spectra, using a home-built matlab routine. In Figure S7 we show the fitting using different peak functions: Gaussian, Lorentz or Pseudo-Voigt functions, which is a linear combination of the first two functions. The parameters extracted from the fitting are reported in Table S2. We also report a fitting without the empirical parameter dA ($dA = 0$). The parameters obtained through the fitting are reported in Table S2. The pseudoVoigt function retraces better the PL and MCPL line shape, revealing a reasonable agreement with the experimental data, despite the significant approximation made in defining the fitting functions. On the other hand, similar line shapes are obtained with different peak functions, indicating the robustness of the fitting procedure.

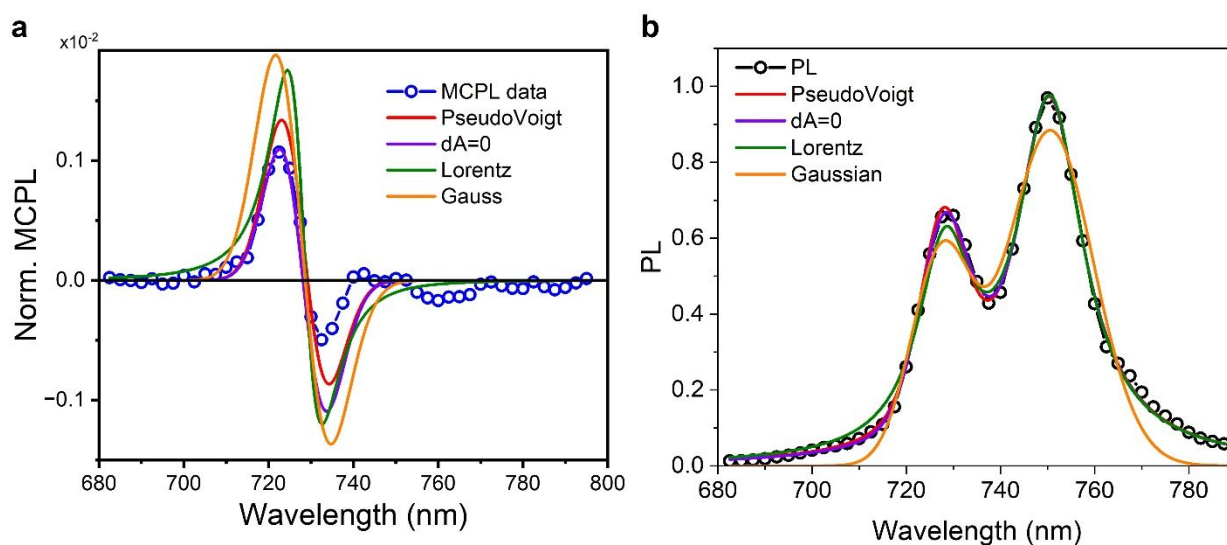


Figure S7. Fitting of normalized MCPL (a) and PL (b) spectra with different peak functions.

Table S2. Parameters extracted from MCPL and PL fitting of the high energy transition using equations S12-S13.

	High energy transition					Low energy transition			
	A	σ (cm ⁻¹)	E (cm ⁻¹)	μ	dA	A	σ (cm ⁻¹)	E (cm ⁻¹)	μ
Pseudo-Voigt function									
Param	0.011	247	13733	0.02	$1.2 \cdot 10^{-5}$	0.058	310	13324	1.00
Error	0.003	12	5	0.50	$0.6 \cdot 10^{-5}$	0.002	13	4	0.07
dA fixed to 0									
Param	0.011	247	13732	0.02	0*	0.058	309	13324	1.00
Error	0.004	14	5	0.54	-	0.002	15	4	0.08
Lorentz function ($\mu=1$)									
Param	0.027	266	13729	1*	$1.9 \cdot 10^{-5}$	0.054	299	13320	1*
Error	0.006	29	11	-	$1.4 \cdot 10^{-5}$	0.004	20	6	-
Gaussian function ($\mu=0$)									
Param	0.022	291	13740	0*	$1.6 \cdot 10^{-5}$	0.044	373	13319	0*
Error	0.010	44	32	-	$2.2 \cdot 10^{-5}$	0.006	41	16	-

* this parameter is kept fixed during the fitting

DC magnetometry

The *dc* magnetic properties of $[\text{Cr}(\text{dqp})_2](\text{PF}_6)_3$ were studied in the 2-300 K temperature range with an applied magnetic field of 1000 Oe. The $\chi_M T$ vs T curve (χ_M is the molar magnetic susceptibility) is shown in Figure S7. The $\chi_M T$ value at room temperature of $1.90 \text{ cm}^3 \text{ mol}^{-1} \text{ K}$ is very close to expected value of $1.875 \text{ cm}^3 \text{ mol}^{-1} \text{ K}$ for a Cr(III) ion with $S = 3/2$ if $g = 2$, which agrees with a quartet ground state (4A_2). Upon cooling, the $\chi_M T$ product remains almost constant until about 10 K and then sharply decreases to reach a value of $1.78 \text{ cm}^3 \text{ mol}^{-1} \text{ K}$ at 2 K.

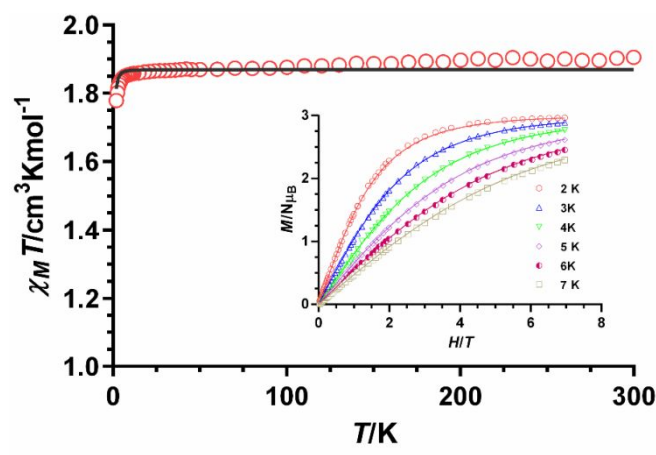


Figure S8. Temperature dependence of χ_{MT} (red circles) and field dependence of the magnetization at 2-7 K (inset). Solid lines represent the best fit to equation.

The field dependence of the magnetization of the Cr(III) compound in the 2-7 K temperature range and magnetic fields ranging from 0 to 7 T have been studied (Figure S7 inset). The magnetization values at 2 K and under the maximum applied field of 7 T of $2.97 N\beta$ match well with the theoretical saturation value of $3 N\beta$ expected for an isolated Cr(III) ion with $g = 2$ and $S = 3/2$.

The magnetic susceptibility and magnetization data were simultaneously fitted using the PHI program⁵ with the ZFS spin Hamiltonian shown in equation 1.

$$\hat{H} = D[\hat{S}_z^2 - S(S+1)/3] + E(\hat{S}_x^2 - \hat{S}_y^2) + \mu_B \sum_{i=x,y,z} g_i \vec{H}_i \cdot \hat{S}_i \quad (\text{eq S10})$$

where the first and second terms account the axial and rhombic magnetic anisotropies, respectively, and the third term represents the Zeeman interaction. To improve the fit of the data and to avoid over-parameterization a term corresponding to the temperature independent paramagnetism (TIP) was included in the above Hamiltonian. It is worth noting that the low accuracy of the magnetic measurements for determining E and $|E/D|$ parameters prevent extracting very reliable ZFS parameters for the Cr(III) compound, particularly the sign of D (the fit of the data is the same with positive and negative D values) and the magnitude of E . In view of these considerations, E was fixed to zero in the fitting procedure. The best fit led to the following magnetic parameters: $|D| = 0.72 \text{ cm}^{-1}$, $g = 1.99$, $\text{TIP} = 0.165 \times 10^{-3} \text{ cm}^3 \text{ mol}^{-1}$ and $R = 2.5 \times 10^{-7}$. It is worth remarking that that magnitude of the D value extracted from the *dc* magnetic data of the compound is very similar to those experimentally and theoretically found for other Cr(III) complexes with slightly distorted octahedral coordination.^{6,7}

HFEPR

HFEPR data analysis and simulation was accomplished using a software package SPIN by A. Ozarowski, freely available at: <https://osf.io/z72tg/>. The same software has a very useful option to calculate the mixing coefficients of the spin sublevels, and their corresponding energies, which is achieved by diagonalizing the spin Hamiltonian matrix containing the ZFS and Zeeman terms. The results of this procedure are shown in Tables S3 and S4.

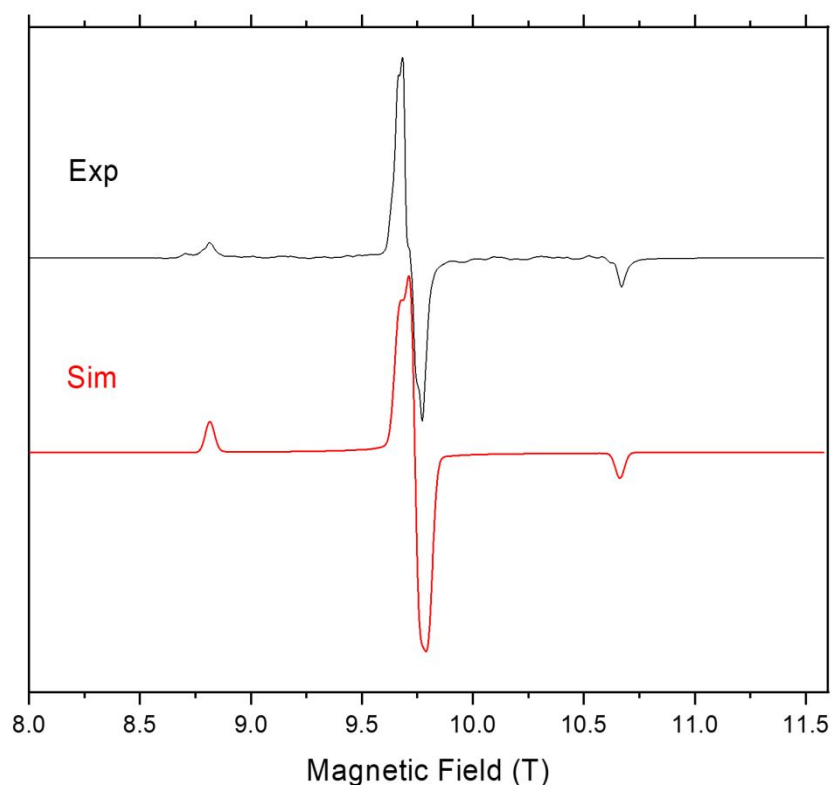


Figure S9. The allowed transitions in the EPR spectrum of $[\text{Cr}(\text{dqp})_2](\text{PF}_6)_3$ constrained as a pellet at 10 K and 270 GHz (black trace) accompanied by their simulation (red trace) using the following spin Hamiltonian parameters: $S = 3/2$, $D = 0.43 \text{ cm}^{-1}$, $E = 0.14 \text{ cm}^{-1}$ ($E/D = 0.325$), $g_x = 1.99$, $g_{y,z} = 1.98$. The simulation assumed a perfectly random orientation of the crystallites in space. The poorly resolved structure on the central line is due to either a deviation from the maximum rhombicity condition ($E/D < 0.33$) or slight g -anisotropy or both.

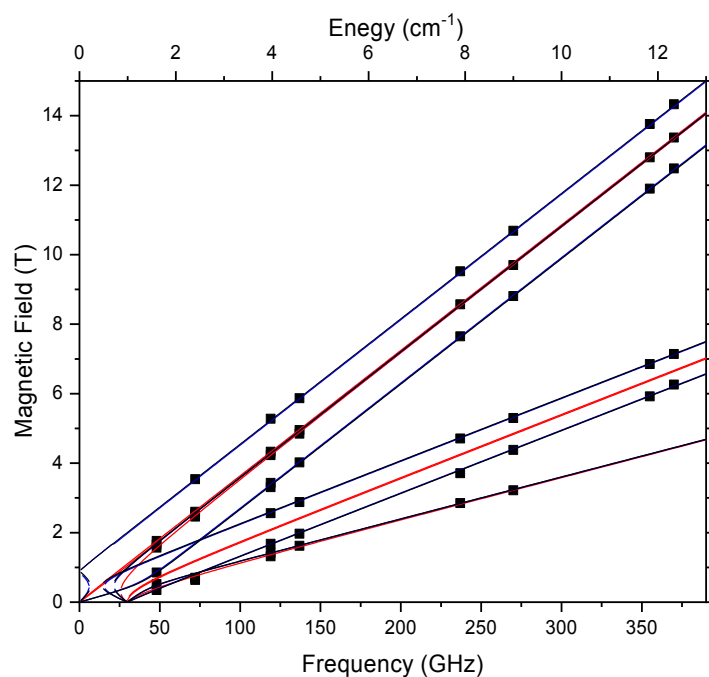


Figure S10. Field vs. frequency map of turning points (squares) in the EPR spectra accompanied by its simulations (curves) using the following best-fitted spin Hamiltonian parameters: $S = 3/2$, $D = -0.436 \text{ cm}^{-1}$, $E = -0.134 \text{ cm}^{-1}$ ($E/D = 0.309$), $g_{iso} = 1.980$. Red curves: magnetic field B_0 parallel to the x-axis of the ZFS tensor; blue: $B_0 \parallel y$; blue: $B_0 \parallel z$.

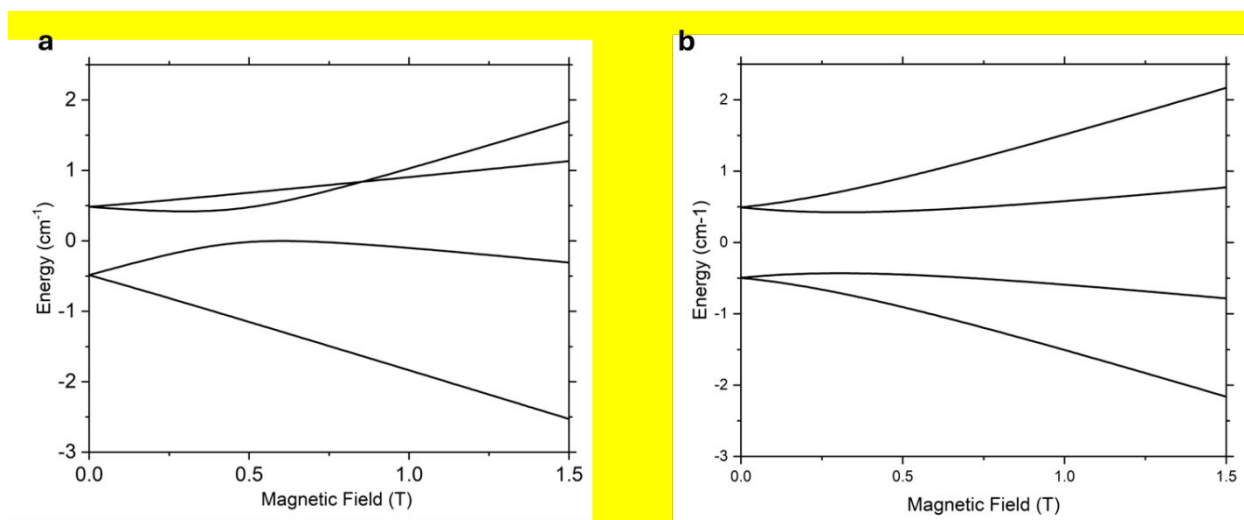


Figure S11. Representation of the HFEPR ground state energy levels for a $S = 3/2$ spin state for the low field region. a: $B_0 \parallel z$, b: $B_0 \parallel x$ (for $B_0 \parallel y$ an almost equivalent situation to case a is obtained, albeit with an inverted level energy order).

Table S3. Energy levels of the spin sublevels of the 4A_2 ground state at 0.4 T (0 is the energy of the unsplit 4A_2 state) and mixing coefficients squared for $B_0 \parallel z$ (an almost equivalent situation is obtained for $B_0 \parallel y$). The first column indicates the main character of the state.

Mixed state	Energy / cm^{-1}	+3/2	+1/2	-1/2	-3/2
$ \widetilde{+1/2}\rangle$	0.66026	0.00000	0.97784	0.00000	0.02215
$ \widetilde{-1/2}\rangle$	0.44380	0.37843	0.00000	0.62157	0.00000
$ \widetilde{+3/2}\rangle$	-0.07031	0.62157	0.00000	0.37843	0.00000
$ \widetilde{-3/2}\rangle$	-1.03375	0.00000	0.022156	0.00000	0.97784

Table S4. Energy levels of the spin sublevels of the 4A_2 ground state at 0.4 T (0 is the energy of the unsplit 4A_2 state) and mixing coefficients squared for $B_0 \parallel x$. The first column indicates the main character of the state.

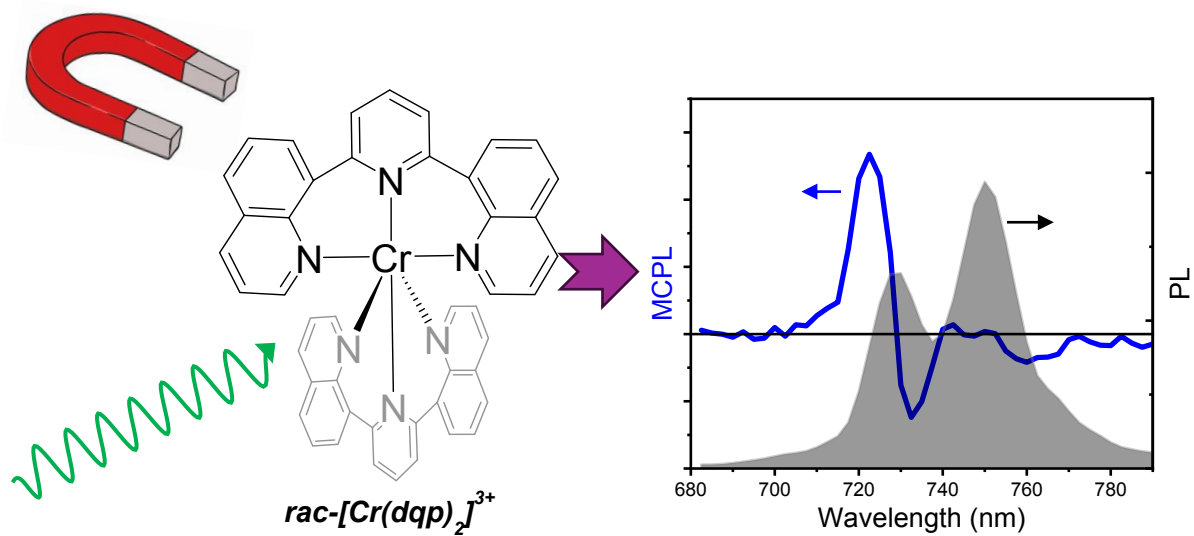
Mixed state	Energy / cm^{-1}	+3/2	+1/2	-1/2	-3/2
$ \pm \widetilde{1/2}\rangle$	0.81387	0.00175	0.49825	0.49825	0.00175
$ \pm \widetilde{1/2}\rangle$	0.43793	0.15025	0.34975	0.34975	0.15025
$ \pm \widetilde{3/2}\rangle$	-0.44038	0.49825	0.00175	0.00175	0.49825
$ \pm \widetilde{3/2}\rangle$	-0.81142	0.34975	0.15025	0.15025	0.34975

Note that at high magnetic field the mixing is negligible and the order (from high to low energy) of the states is $|\pm 3/2\rangle$, $|\pm 1/2\rangle$, $|\pm 1/2\rangle$, $|\pm 3/2\rangle$.

References

- 1 J.-R. Jiménez, B. Doistau, C. M. Cruz, C. Besnard, J. M. Cuerva, A. G. Campaña and C. Piguet, *J. Am. Chem. Soc.*, 2019, **141**, 13244–13252.
- 2 A. K. Hassan, L. A. Pardi, J. Krzystek, A. Sienkiewicz, P. Goy, M. Rohrer and L.-C. Brunel, *J. Magn. Reson.*, 2000, **142**, 300–312.
- 3 S. Lenz, H. Bamberger, P. P. Hallmen, Y. Thiebes, S. Otto, K. Heinze and J. van Slageren, *Phys. Chem. Chem. Phys.*, 2019, **21**, 6976–6983.
- 4 P. E. Hoggard, *Zeitschrift für Naturforschung A*, 1981, **36**, 1276–1288.
- 5 N. F. Chilton, R. P. Anderson, L. D. Turner, A. Soncini and K. S. Murray, *J. Comput. Chem.*, 2013, **34**, 1164–1175.
- 6 G. Elbers, S. Remme and G. Lehmann, *Inorg. Chem.*, 1986, **25**, 896–897.
- 7 D. G. Liakos, D. Ganyushin and F. Neese, *Inorg. Chem.*, 2009, **48**, 10572–10580.

Magnetic circularly polarized luminescence of spin-flip transitions of a Cr(III) complex is measured at low field.



The data supporting this article have been included as part of the Supplementary Information

ARTICLE

Magnetic circularly polarized luminescence from spin flip transitions in a molecular Ruby

Received 00th January 20xx,
Accepted 00th January 20xx

DOI: 10.1039/x0xx00000x

Alessio Gabbani,^{a,b} Maxime Poncet,^c Gennaro Pescitelli,^a Laura Carbonaro,^a J. Krzystek,^d Enrique Colacio,^e Claude Piguet,^c Francesco Pineider,^{a,b} Lorenzo Di Bari,^a Juan-Ramón Jiménez*,^e Francesco Zinna*^a

Magnetic circularly polarized luminescence (MCPL), i.e. the possibility of generating circularly polarized luminescence in the presence of a magnetic field in achiral or racemic compounds, is a technique of rising interest. Here we show that the far-red spin-flip (SF) transitions of a molecular Cr(III) complex give intense MCD (magnetic circular dichroism) and in particular MCPL (g_{MCPL} up to $6.3 \cdot 10^{-3} \text{ T}^{-1}$) even at magnetic fields as low as 0.4 T. Cr(III) doublet states and SF emission are nowadays the object of many investigations, as they may open the way to several applications. Due to their nature, such transitions can be conveniently addressed by MCPL, which strongly depends on the zero field splitting and Zeeman splitting of the involved states. Despite the complexity of the nature of such states and the related photophysics, the obtained MCPL data can be rationalized consistently with the information recovered with more established techniques, such as HFEPR (high-frequency and -field electron paramagnetic resonance). We anticipate that emissive molecular Cr(III) species may be useful in magneto-optical devices, such as magnetic CP-OLEDs.

Introduction

Molecular complexes based on d-metals offer a diverse and intriguing photophysics,¹ with applications ranging from photocatalysis,² optoelectronics,^{3,4} imaging^{5,6} and photodynamic therapy.^{7–9} To understand the often non-trivial photophysics at play, the use of less common spectroscopic techniques may be beneficial. In turn, this is necessary to exploit the full potential of those systems and to give indications for a rational design of the ligands and complexes.

A particularly interesting case is observed when metal-centred excited states differ only by spin configuration with respect to the ground state.¹⁰ Such configurations are called spin-flip (SF) states and they may display sharp phosphorescent transitions (SF-transitions), forbidden by electric transition moment, with lifetimes up to a millisecond. SF luminescence was observed in the case of

V(II)/V(III),^{11–13} Mn(IV),^{14,15} Mo(III),^{16,17} Re(IV),¹⁷ and in particular, remarkable results in terms of emission efficiency were obtained in the case of (pseudo)octahedral Cr(III) complexes.^{18–20} Such complexes show luminescence associated with the doublet states $^2T_1/2E$ (Figure 1) with quantum yields up to 30% with narrow bands in the far red or near infrared region.¹⁸ These features, reminiscent of those of the ruby gemstone, can be obtained in a molecular compound with octahedral-like geometry (i) to avoid excited state distortions and (ii) to induce strong ligand field splitting, needed to shift the 4T_2 states toward higher energy thus preventing deactivation of the SF states due to back intersystem crossing (BISC).¹⁹ Complexes featuring SF states may be exploited as optical probes for oxygen²⁰, pressure²¹ and temperature,²² photocatalysis^{23–25} and photocathodic solar cells.^{19,26}

Concerning the luminescence activity associated with the SF transitions, the most promising results have been achieved so far by employing two families of Cr(III) complexes: $[\text{Cr}(\text{ddpd})_2]^{3+}$ (ddpd = N,N'-dimethyl-N,N''-dipyridin-2-ylpyridine-2,6-diamine)^{18,27,28} and $[\text{Cr}(\text{dqp})_2]^{3+}$ (dqp = 2,6-di(quinolin-8-yl)pyridine).^{29,30} In those cases, the first coordination sphere is roughly octahedral, but the arrangement of the tridentate organic ligand around the Cr-center defines a λ/δ chirality in an overall D_2 geometry.³¹ Thanks to the electric dipole forbidden nature of the SF transition, in enantiopure form, such compounds display highly circularly polarized luminescence (CPL), with dissymmetry factors (g_{lum}) on the order of 10^{-1} .^{30–34} Such values are comparable with those obtained for the $f-f$ transitions of chiral lanthanide(III) complexes,^{35–39} but Cr offers the advantage of being cheaper, kinetically inert and more abundant than lanthanides.⁴⁰

^a Dipartimento di Chimica e Chimica Industriale, University of Pisa, via Moruzzi 13, 56124, Pisa, Italy

^b Department of Physics and Astronomy, University of Florence, via Sansone 1, 50019, Sesto Fiorentino, Italy

^c Department of Inorganic and Analytical Chemistry, University of Geneva, 30 quai E. Ansermet, CH-1211 Geneva 4, Switzerland

^d National High Magnetic Field Laboratory, Florida State University, Tallahassee, Florida 32310, USA

^e Departamento de Química Inorgánica, Facultad de Ciencias, University of Granada and "Unidad de Excelencia en Química (UEQ)", Avda. Fuente Nueva s/n, 18071, Granada, Spain.

E-mail:

jrijimenez@ugr.es, francesco.zinna@unipi.it

Electronic Supplementary Information (ESI) available: [details of any supplementary information available should be included here]. See DOI: 10.1039/x0xx00000x

ARTICLE

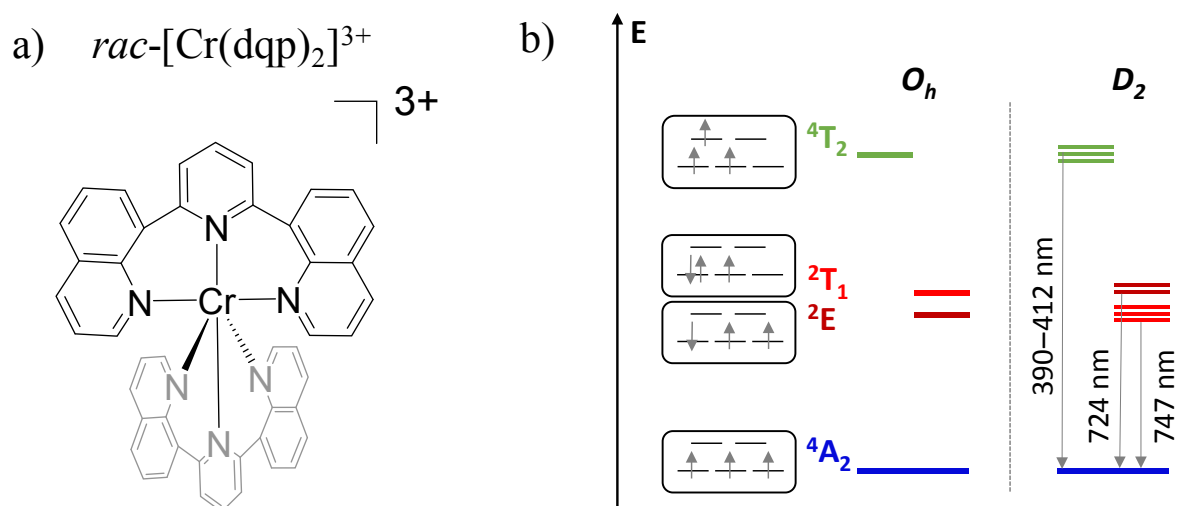


Figure 1. a. Structure of the complex. b. Electronic states of $[\text{Cr}(\text{dqp})_2]^{3+}$ in an ideal octahedral (O_h) and D_2 geometry; Note the ${}^2T_1/{}^2E$ level inversion from O_h to D_2 geometry.

A different technique to study the circular polarization of the emitted light is magnetic CPL (MCPL), where the physical origin of the CP emission is not the chirality of the material, but the effect is triggered by the application of an external magnetic field. This technique belongs to the family of magneto-optical spectroscopies, along with the more common Faraday rotation and magnetic circular dichroism (MCD).^{41–43} In a MCPL experiment, the circular polarization of the luminescence is studied, when the sample is placed under a magnetic field collinear with the emission direction, and excited with unpolarized light.^{44,45} Unlike CPL, MCPL may be displayed by both chiral and achiral luminescent systems and it does not depend on the enantiomer chirality. Indeed, CPL and MCPL follow very different selection rules. CPL is gauged by the scalar product $\mathbf{m}_{ng} \cdot \boldsymbol{\mu}_{gn}$, where \mathbf{m} and $\boldsymbol{\mu}$ are the magnetic and electric transition moments between the ground state g and excited state(s) n .⁴⁶ On the other hand, several mechanisms can lead to MCPL. Relatively strong signals are predicted in the case of orbital or spin degenerate ground or excited states, where the degeneracy is removed by the magnetic field due to the Zeeman effect. In these cases, the MCPL signal depends on $\mathbf{m}_{gg} \cdot \boldsymbol{\mu}_{ng} \boldsymbol{\mu}_{gn}$ and $\mathbf{m}_{nn} \cdot \boldsymbol{\mu}_{ng} \boldsymbol{\mu}_{gn}$ products (\mathbf{m}_{gg} and \mathbf{m}_{nn} are the static magnetic dipole moments of the ground and excited state), for a degenerate ground or excited state respectively.^{47,48} Those expressions are associated to the so-called Faraday A- and C-terms.^{44,47,49,50} Emitting compounds characterized by a strong spin-orbit coupling, which allows for a significant mixing of states, are good candidates for magnetooptical spectroscopies, including MCPL.

MCPL has been thus studied in the case of f - f transitions of lanthanide complexes,^{51–53} d -metals (such as Ru and Ir

complexes),^{54,55} organic and metallo-organics compounds.^{56–64} MCPL and MCD were also reported in early studies of Cr(III) inorganic structures.^{65,66} MCD was also used to study far red/near infrared (NIR) transitions in the case of Ir or Pt complexes,^{67,68} where their observation through emission, and thus MCPL, is challenging. On the other hand, emissive Cr(III) compounds are potentially a more suitable platform to address metal transitions through MCPL. On a fundamental level, an analysis of the MCPL spectrum can elucidate the nature of the excited and ground states, Zeeman effects, etc., and along with other techniques can help to understand the full picture of the photophysics of a complex system.⁴⁴ Moreover, MCPL-active compounds have recently found applications in OLEDs able to emit circularly polarized electroluminescence in a magnetic field (MCP-OLEDs),^{69–72} therefore there is also a practical interest in unveiling different types of emitters endowed with significant MCPL. In the following, we investigate the racemic $[\text{Cr}(\text{dqp})_2](\text{PF}_6)_3$ material by MCPL and MCD (Figure 1b). As introduced above, $[\text{Cr}(\text{dqp})_2]^{3+}$ is one of the archetypes of a molecular ruby and the same concept shown here may be applied to similar systems.

Results and Discussion

Optical and magneto-optical studies reported here were performed on deaerated acetonitrile solutions of the racemic compound $[\text{Cr}(\text{dqp})_2](\text{PF}_6)_3$. The photoluminescence (PL) spectrum of $[\text{Cr}(\text{dqp})_2]^{3+}$ shows two main emission bands centred at 750 and 729 nm (Figure 2), associated to the SF transitions (${}^2E/{}^2T_1 \rightarrow {}^4A_2$) from the sublevels of the doublet excited states (see Figure 1a) to the ground

state. The lower energy band appears more intense than the higher energy one by a factor of 1.53 at 300 K, due to a higher Boltzmann population with an energy gap of $\approx 420\text{ cm}^{-1}$ between the two bands.²⁷

We measured the MCPL emission at 300 K under a magnetic field of $\pm 0.4\text{ T}$ generated by a permanent magnet, exciting the sample at 365 nm (see the ESI and Figure S1 for the details of the measurement set-up). In these conditions, a relatively strong and slightly asymmetric bisignate MCPL band was observed corresponding to the higher energy doublet transition (Figure 2). Such band has a cross-over point at 725 nm, matching the maximum of the corresponding photoluminescence band. This derivative-like shape is consistent with a signal originating from Zeeman-split states (see below). The MCPL strength can be quantified by a magnetic field (H) normalized dissymmetry factor (g_{MCPL}), defined as:

$$g_{\text{MCPL}} = 2 \frac{1(I_L - I_R)}{H(I_L + I_R)} \quad \text{Eq. 1}$$

where I_L and I_R are the left and right circularly polarized components of the emission under the magnetic field. In our case, we found a g_{MCPL} of $6.3 \cdot 10^{-3}\text{ T}^{-1}$ at 722 nm and $-2.1 \cdot 10^{-3}\text{ T}^{-1}$ at 733 nm. These values are in line with those obtained for other *d* or *f*-metal complexes.^{52–54,73} A much weaker ($\approx 0.9 \cdot 10^{-3}\text{ T}^{-1}$) band around 750 nm associated the lower energy SF transition was also observed. As expected, roughly mirror image MCPL spectra were obtained for \pm magnetic field (Figure S3a), by reversing the orientation of the permanent magnet. In Figure 2, we report the MCPL as the semi-difference of the polarized signal S obtained under positive ($S(+)$) and negative ($S(-)$) H, as:

$$\text{MCPL} = \frac{1}{2}[S(+)-S(-)] \quad \text{Eq. 2}$$

Positive and negative fields are here defined as parallel and anti-parallel to the k -vector, i.e. the propagating direction of light. Baseline effects and possible artefact signals due to photoselection cause some deviation from the mirror image relationship expected for spectra obtained under opposite magnetic field, especially in the case of small signals (Figure S3a). The data treated according to Eq. 2 ensures that such artefacts, which are magnetic field-independent, are eliminated and only the true MCPL is recovered (Figure S3b).

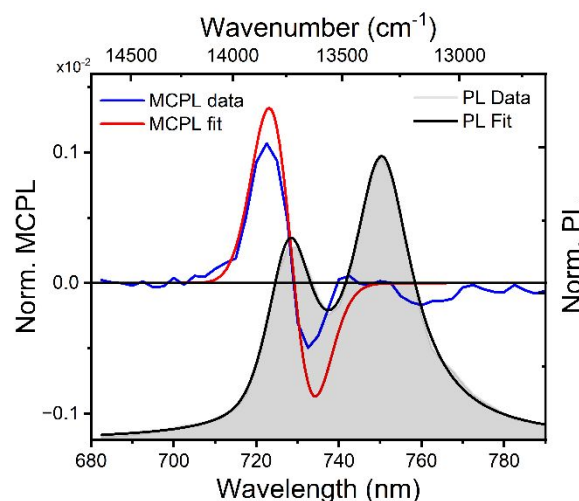


Figure 2. PL and MCPL at 0.4 T, normalized for the PL maximum, of the Cr^{3+} complex dissolved in deaerated acetonitrile, along with the corresponding fittings according to the rigid-shift model (see the text).

The same SF transitions were also studied in absorption through MCD, on a concentrated solution of the complex under $\pm 1.4\text{ T}$ magnetic field (Figure 3b), generated by an electromagnet. A derivative-like signal was observed associated to the higher energy doublet transition, similar to the corresponding MCPL band. No significant MCD corresponding to the lower energy SF transition was detected. Similarly to the MCPL, MCD dissymmetry factor (g_{MCD}) can be defined as:

$$g_{\text{MCD}} = 2 \frac{1(A_L - A_R)}{H(A_L + A_R)} \quad \text{Eq. 3}$$

With A_L (A_R) the absorbance of left (right) circularly polarized light. The g_{abs} were estimated approximately $+1.7$ and $-1.4 \cdot 10^{-2}\text{ T}^{-1}$ at 725 and 728 nm respectively. Such values are 2 orders of magnitude higher than those observed for the MCD bands observed between 500 and 250 nm (Figure 3 a), associated with the ligand-centred (LC) and ligand-to-metal charge-transfer transitions ($g_{\text{MCD}} \approx 1 \cdot 10^{-4}\text{ T}^{-1}$). This confirms that magneto-optical techniques are excellent tools to study SF transitions. Such studies are particularly challenging in standard absorption spectroscopy experiments due to the very weak extinction coefficient of SF transitions (below $1\text{ M}^{-1}\text{ cm}^{-1}$, see Figure 3b), which requires high concentrations and deconvolution from the tail of the high energy absorption transitions, making it difficult to distinguish the extinction peaks from the instrumental noise. On the other hand, we show here that MCD experiments can give signals well above the instrumental noise, without the need for deconvolution procedures. As expected, the MCD signal intensity was found to be linear with the applied field H (Figure S4). The overall similarity of the MCD and MCPL shape and signature is consistent with minor structural differences between the ground state and the doublet states of Cr(III) . Indeed, SF states have a nested nature and therefore they are expected to be only weakly distorted with respect to the ground state.^{10,23}

To rationalize these results, it is worth analysing the states involved in the SF transitions giving origin to the MCD and MCPL spectra. In the complex, the presence of the helically twisted tridentate dqg suppresses any symmetry plane and lowers the overall symmetry to D_2 . In such symmetry, the orbital degeneracy of the excited states is removed, and 2T_1 and 2E states are split into 3 and 2 components respectively (Figure 1a). The main MCPL signal at 729 nm is associated with the lower component of the doubly degenerate 2E state. A small contribution to the PL, giving non-significant MCPL, is observed at approximately 710 nm, possibly stemming from the higher energy component of the 2E state (Figure S2). Moreover, even in the absence of an external field, the orbitally-nondegenerate quartet ground state (4A_2) is split by the zero-field splitting (ZFS) into two Kramers doublets (KD) $|\pm 1/2\rangle$ and $|\pm 3/2\rangle$ (Figure 4).

To extract the ZFS and the corresponding spin Hamiltonian D and E parameters, we followed the method proposed by van Slageren *et*

al. (see ESI).⁷⁴ As the first step, the energies corresponding to the 3 $^4A_2 \rightarrow ^4T_2$ term-to-term transitions were determined by a phenomenological deconvolution of the 360–500 nm region of the MCD spectrum (Figure S5). With this procedure, we identified the following energies, centred approximately at 24220, 24922 and 25630 cm^{-1} (Table S1). From these values (see ESI for the formulae in a D_2 geometry), we calculated D and E parameters as approximately 0.51 and 0.16 cm^{-1} , respectively, with a rhombicity factor $E/D=0.32$, close to the maximum (1/3). The corresponding ZFS was calculated to be $\approx 1.1 \text{ cm}^{-1}$ as $2\sqrt{D^2 + 3E^2}$ (see Figure 4). Despite the large error of the method (see for instance the standard errors on the fitting coefficient in Table S1), the values are comparable with those found for the analogue complex $[\text{Cr}(\text{ddpd})_2]^{3+}$,⁷⁴ and the values found by HFEPR (high-frequency and -field electron paramagnetic resonance) on our complex (see below).

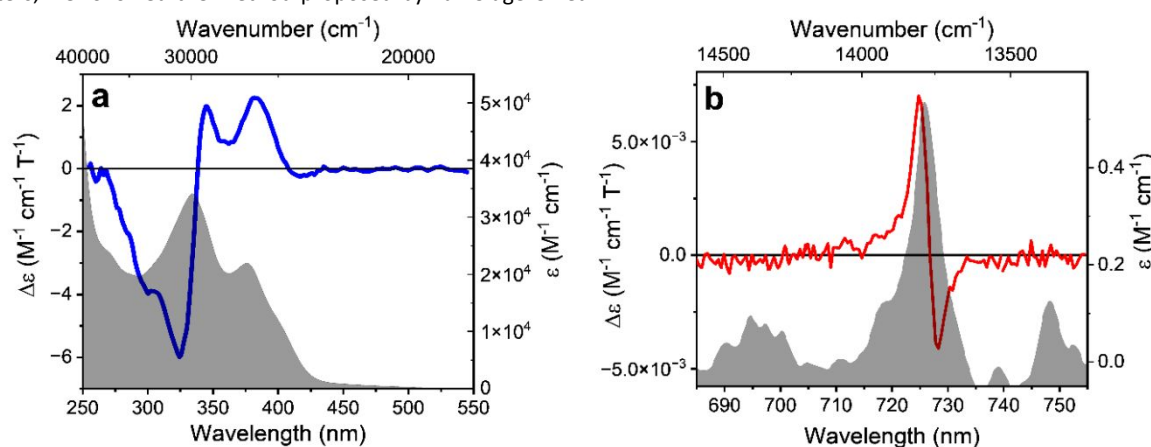


Figure 3. MCD and extinction spectra of an acetonitrile solution of $[\text{Cr}(\text{dqg})_2]^{3+}$, for the higher energy region (a) and for the SF transition region (b). The data are normalized for concentration, optical path and applied magnetic field.

We now focus our analysis on the MCPL and PL spectra at the NIR SF transitions. In the presence of an external magnetic field, the degeneracy of the KDs of the quartet ground states is removed by Zeeman effect giving 4 spin states: ideally $|+1/2\rangle$, $|-1/2\rangle$, $|+3/2\rangle$ and $|-3/2\rangle$. Similarly, the doublet excited states split into $|+1/2\rangle$ and $|-1/2\rangle$ states.

In the following, we focus only on the higher energy SF band around 729 nm, producing the main signal. In a reasonably simplified scheme, we consider only the transitions among Zeeman levels with $\Delta M_s = \pm 1$.⁷⁵ A $\Delta M_s > 0$ corresponds to a positive MCPL transition and vice versa, therefore a total of two closely spaced positive and two negative MCPL contributions are expected (Figure 4).

When the bands are separated by an energy much smaller than the bandwidth, the spectral features can be conveniently modelled by using the so-called rigid-shift approximation. This method is usually applied to model A- and C-Faraday terms in MCD.^{43,76,77} Within this model, PL and MCPL spectra are fitted simultaneously using a home-built MATLAB code, employing fitting functions that hold shared parameters. The emission is fitted with a bell-shaped function centred on the energy barycentre (unsplit levels), while the MCPL is

fitted with equal but opposite functions, displaced by the small field-induced splitting (see ESI and Figure S6). All the functions, used for both the PL and MCPL, share the same shape and bandwidth, and are therefore determined simultaneously in the fitting. To carry out this procedure, we used the four energy levels of the 4A_2 state determined by HFEPR at 0.4 T (see below), as fixed parameters. The fitting obtained through this model, by using pseudo-Voigt functions, closely retraces the experimental PL and MCPL data (Figure 2 and ESI). Similar results were obtained using purely Gaussian or Lorentzian functions, but pseudo-Voigt functions retrace better the PL and MCPL line shapes (Figure S7 and Table S2). The overestimation of the model with respect to the experimental MCPL data may be due to the fact that, in the case of ZFS with $E \neq 0$, the four states associated with 4A_2 cannot be described by a pure M_s quantum number as they are significantly mixed (see below). This would therefore impact the underlying assumption that each transition is completely circularly polarized. Notice that the lifetime of the excited state being sufficiently long ($\tau_{\text{obs}} = 1.2 \text{ ms}$),³³ the population of its Zeeman levels follows Boltzmann distribution. The Zeeman splitting being much smaller than room temperature thermal energy (207 cm^{-1} at 298 K), the Zeeman levels of the doublet excited states are almost

equally populated, as $1 - (\Delta E/k_b T) \approx 0.998$. Figure 4 quantitatively summarizes the fine structure of the electronic level involved in the MCPL emission of the main band.

To corroborate the analysis and demonstrate the consistency of our approach, we performed magnetometry and EPR characterization. DC magnetometry, studied in the 2–300 K temperature range, confirms a quartet ground state (4A_2 , see supporting information and Figure S8). Saturation magnetization at 2 K is consistent with what expected for isolated Cr(III) cations with $g=2$ and $S=3/2$. Upon cooling, the $\chi_M T$ product remains almost constant until about 10 K and then sharply decreases to reach a value of $1.78 \text{ cm}^3 \text{ mol}^{-1} \text{ K}$ at 2 K. This decrease is due to the ZFS and Zeeman interactions. The simultaneous fitting of the susceptibility and magnetization data with the ZFS Hamiltonian using the PHI Software⁷⁹ leads to a $|D|$ value of 0.72 cm^{-1} , which is rather consistent with the values extracted from MCD and HFEPR spectroscopies.

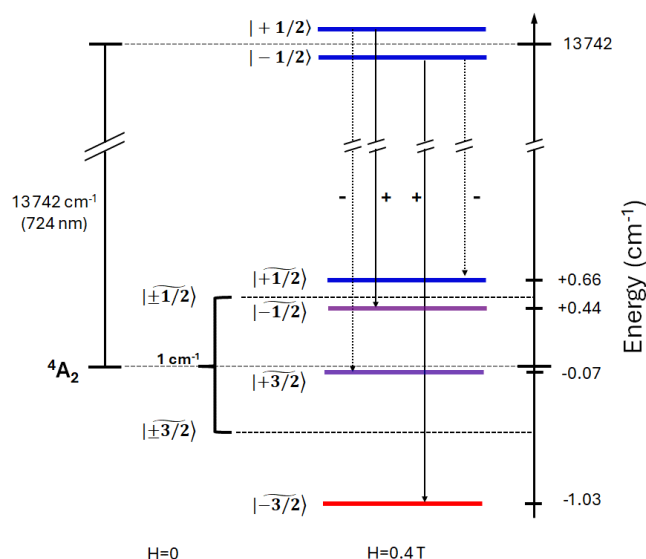


Figure 4. ZFS- and Zeeman-split levels at 0.4 T corresponding to the main MCPL bands. The MCPL transitions are represented by the dotted arrows along with the expected sign. The + and – symbols indicate left and right circularly polarized emissive transitions respectively. The energies of ground state sublevels (for $B_0 \parallel z$) are obtained through HFEPR analysis (see Figure 5 and Table S3). As considerable mixing occurs (see Table S3), the predominant character of the M_S state is indicated by a \sim symbol. Purple colour indicates strongly mixed states.

To confirm the determined D and E values from MCD measurements, the Cr(III) compound was studied by HFEPR spectroscopy.⁸⁰ The shape and amplitude of the low-temperature (30 K) spectra of the powder sample “as is” (i.e. unconstrained) strongly suggested field-induced alignment (i.e. torquing) of the crystallites. Indeed, the resulting spectra could be very well simulated as originating from a single crystal oriented with the z -axis of the ZFS tensor parallel to the magnetic field B_0 (Figure 5). At 270 GHz, the three dominating peaks between 8 and 12 T represent the allowed $\Delta M_S = \pm 1$ transitions

between the spin sublevels of the $S = 3/2$ spin state of Cr(III). The weak peaks in the 3–6 T range are the nominally forbidden $\Delta M_S = \pm 2$ and ± 3 transitions. The structure visible on the peaks is an artefact that can be attributed to imperfect field alignment and is not simulated.

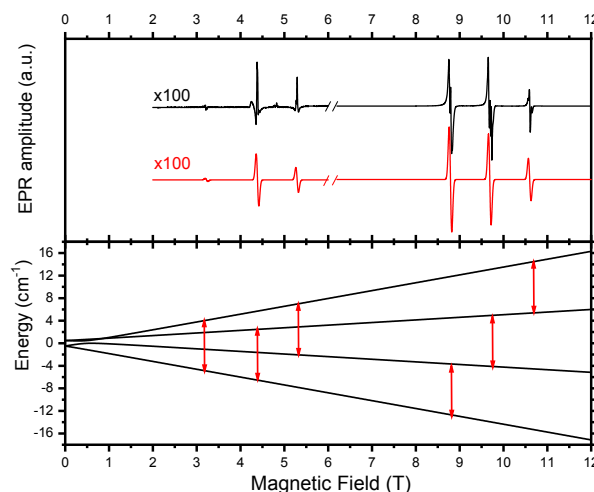


Figure 5. Top: EPR spectrum of a polycrystalline sample containing the Cr(III) compound at 30 K and 270 GHz (black trace) accompanied by its simulation (red trace) using the following spin Hamiltonian parameters: $S = 3/2$, $D = 0.42 \text{ cm}^{-1}$, $E = 0.14 \text{ cm}^{-1}$ ($E/D = 0.33$, maximum rhombicity limit), $g_{\text{iso}} = 1.99$. The simulation assumed a single crystal oriented with the z -axis of the ZFS tensor parallel to the magnetic field B_0 . Bottom: Representation of the energy levels for a $S = 3/2$ spin state at 270 GHz. The HFEPR transitions between the spin sublevels are marked with red arrows.

In order to extract the full set of frequency-independent spin Hamiltonian parameters, the sample was constrained using n -eicosane and pressed into a pellet (Figure S9). The resulting spectrum is accompanied by a simulation, this time assuming a powder distribution of the crystallites in space. The simulation parameters are modified relative to those used above to account for the slight asymmetry of the central line: $D = 0.43 \text{ cm}^{-1}$, $E = 0.14 \text{ cm}^{-1}$ ($E/D = 0.325$), $g_x = 1.99$, $g_{y,z} = 1.98$.

To finalize the values of frequency-independent spin Hamiltonian parameters, we built a two-dimensional map of turning points in pellet spectra and applied the tunable-frequency methodology⁸¹ by fitting the parameters simultaneously to that map. This resulted in the following values: $D = -0.436(7) \text{ cm}^{-1}$, $E = -0.144(7) \text{ cm}^{-1}$ ($E/D = 0.31$), $g_{\text{iso}} = 1.980(4)$ (Figure S10). The negative sign of D reproduced single-frequency spectra better than a positive value.

Altogether, these results are in good agreement with the ones that we found by MCPL and MCD experiments. Finally, the nature of the M_S states associated with 4A_2 was evaluated by calculating the mixing coefficients at 0.4 T (Table S3, S4, see also Figure S11 for an expansion of HFEPR levels at low field). The coefficients show (in the case of $B_0 \parallel z$, see Table S3) a strong mixing between two inner $|+3/2\rangle$ and $|-1/2\rangle$ levels, responsible for the avoided level crossing

near 1 T visible in Figure 5 (bottom), while the outer levels retain mostly their $|+1/2\rangle$ and $|-3/2\rangle$ character.

Conclusions

Beyond the many areas of interest in Cr(III) SF transitions of the molecular ruby $[\text{Cr}(\text{dqp})_2]^{3+}$, we show here that they also display a strong MCPL activity. MCD and MCPL techniques are here applied to elucidate the fine structure of the levels involved in the SF transitions. In particular, the analysis of SF transition through MCPL was consistent with the energies found with the more established EPR spectroscopy. Such possibilities offered by magneto-optical techniques can be exploited to gather more insight into the photophysics of SF transitions in related cases, e.g. in view of optical read-out of molecular qubits. Moreover, it opens up new opportunities such as applications in magneto-optical and magnetoelectronic devices.

Author Contributions

Conceptualization: F.Z.; Data curation: A.G., G.P., F.P., J.R.J., F.Z.; Formal Analysis: A.G., F.Z.; Resources: M.P., C.P., J.R.J.; Funding acquisition: L.D.B., C.P., F.P., J.R.J.; Investigation: A.G., L.C., E.C., J.K., F.Z. Methodology: F.Z., G.P. Writing – original draft: A.G., J.R.J., F.Z.; Writing – review & editing: all authors.

Conflicts of interest

There are no conflicts to declare.

Acknowledgements

We would like to thank Mr David Michelotti for technical support with the MCPL set-up. F.P. acknowledges MUR through PRIN-PNRR project (P20229723Z) J.R.J. thanks Ministerio de Ciencia Innovación y Universidades for a Ramón y Cajal contract (grant RYC2022-037255-I) funded by MCIN/AEI/10.13039/501100011033 and FSE+. Part of this work was done at the National High Magnetic Field Laboratory which is funded by the US National Science Foundation (Cooperative Agreement DMR-212856) and the State of Florida. Dr. A. Ozarowski (NHMFL) is acknowledged for his EPR fit and simulation software SPIN and help with solving the level mixing problem. Prof. L. Sorace (University of Florence) is acknowledged for fruitful discussions.

Notes and references

- V. Balzani, A. Credi and M. Venturi, *Coord. Chem. Rev.*, 1998, **171**, 3–16.
- J. Twilton, C. (Chip) Le, P. Zhang, M. H. Shaw, R. W. Evans and D. W. C. MacMillan, *Nat Rev Chem*, 2017, **1**, 1–19.
- H. Xu, R. Chen, Q. Sun, W. Lai, Q. Su, W. Huang and X. Liu, *Chem. Soc. Rev.*, 2014, **43**, 3259–3302.
- W. C. H. Choy, W. K. Chan and Y. Yuan, *Adv. Mater.*, 2014, **26**, 5368–5399.
- M. P. Coogan and V. Fernández-Moreira, *Chem. Commun.*, 2013, **50**, 384–399.
- J. Berrones Reyes, M. K. Kuimova and R. Vilar, *Curr. Opin. Chem. Biol.*, 2021, **61**, 179–190.
- Y. Wu, S. Li, Y. Chen, W. He and Z. Guo, *Chem. Sci.*, 2022, **13**, 5085–5106.
- T. W. Rees, P.-Y. Ho and J. Hess, *ChemBioChem*, 2023, **24**, e202200796.
- C. B. Smith, L. C. Days, D. R. Alajroush, K. Faye, Y. Khodour, S. J. Beebe and A. A. Holder, *Photochem. Photobiol.*, 2022, **98**, 17–41.
- W. R. Kitzmann, J. Moll and K. Heinze, *Photochem Photobiol Sci*, 2022, **21**, 1309–1331.
- M. Dorn, J. Kalmbach, P. Boden, A. Kruse, C. Dab, C. Reber, G. Niedner-Schatteburg, S. Lochbrunner, M. Gerhards, M. Seitz and K. Heinze, *Chem. Sci.*, 2021, **12**, 10780–10790.
- M. Dorn, D. Hunger, C. Förster, R. Naumann, J. van Slageren and K. Heinze, *Chem. Eur. J.*, 2023, **29**, e202202898.
- M. Dorn, J. Kalmbach, P. Boden, A. Pöpcke, S. Gómez, C. Förster, F. Kuczelinis, L. M. Carrella, L. A. Büldt, N. H. Bings, E. Rentschler, S. Lochbrunner, L. González, M. Gerhards, M. Seitz and K. Heinze, *J. Am. Chem. Soc.*, 2020, **142**, 7947–7955.
- J. P. Harris, C. Reber, H. E. Colmer, T. A. Jackson, A. P. Forshaw, J. M. Smith, R. A. Kinney and J. Telser, *Can. J. Chem.*, 2017, **95**, 547–552.
- N. R. East, R. Naumann, C. Förster, C. Ramanan, G. Diezemann and K. Heinze, *Nat. Chem.*, 2024, 1–8.
- W. R. Kitzmann, D. Hunger, A.-P. M. Reponen, C. Förster, R. Schoch, M. Bauer, S. Feldmann, J. van Slageren and K. Heinze, *Inorg. Chem.*, 2023, **62**, 15797–15808.
- Q. Yao and A. W. Maverick, *Inorg. Chem.*, 1988, **27**, 1669–1670.
- C. Wang, S. Otto, M. Dorn, E. Kreidt, J. Lebon, L. Sršan, P. Di Martino-Fumo, M. Gerhards, U. Resch-Genger, M. Seitz and K. Heinze, *Angew. Chem. Int. Ed.*, 2018, **57**, 1112–1116.
- S. Treiling, C. Wang, C. Förster, F. Reichenauer, J. Kalmbach, P. Boden, J. P. Harris, L. M. Carrella, E. Rentschler, U. Resch-Genger, C. Reber, M. Seitz, M. Gerhards and K. Heinze, *Angew. Chem. Int. Ed.*, 2019, **58**, 18075–18085.
- C. Wang, S. Otto, M. Dorn, K. Heinze and U. Resch-Genger, *Anal. Chem.*, 2019, **91**, 2337–2344.
- S. Otto, J. P. Harris, K. Heinze and C. Reber, *Angew. Chem. Int. Ed.*, 2018, **57**, 11069–11073.
- S. Otto, N. Scholz, T. Behnke, U. Resch-Genger and K. Heinze, *Chem. Eur. J.*, 2017, **23**, 12131–12135.
- W. R. Kitzmann and K. Heinze, *Angew. Chem. Int. Ed.*, 2023, **62**, e202213207.
- T. H. Bürgin, F. Glaser and O. S. Wenger, *J. Am. Chem. Soc.*, 2022, **144**, 14181–14194.
- C. Wang, H. Li, T. H. Bürgin and O. S. Wenger, *Nat. Chem.*, 2024, 1–9.
- B. Doistau, G. Collet, E. A. Bolomey, V. Sadat-Noorbakhsh, C. Besnard and C. Piguet, *Inorg. Chem.*, 2018, **57**, 14362–14373.
- S. Otto, M. Grabolle, C. Förster, C. Kreitner, U. Resch-Genger and K. Heinze, *Angew. Chem. Int. Ed.*, 2015, **54**, 11572–11576.
- S. Otto, C. Förster, C. Wang, U. Resch-Genger and K. Heinze, *Chem. Eur. J.*, 2018, **24**, 12555–12563.
- J.-R. Jiménez, M. Poncet, B. Doistau, C. Besnard and C. Piguet, *Dalton Trans.*, 2020, **49**, 13528–13532.
- J.-R. Jiménez, B. Doistau, C. M. Cruz, C. Besnard, J. M. Cuerva, A. G. Campaña and C. Piguet, *J. Am. Chem. Soc.*, 2019, **141**, 13244–13252.
- M. Poncet, A. Benchohra, J.-R. Jiménez and C. Piguet, *ChemPhotoChem*, 2021, **5**, 880–892.

- 32 C. Dee, F. Zinna, W. R. Kitzmann, G. Pescitelli, K. Heinze, L. D. Bari and M. Seitz, *Chem. Commun.*, 2019, **55**, 13078–13081.
- 33 J.-R. Jiménez, M. Poncet, S. Míguez-Lago, S. Grass, J. Lacour, C. Besnard, J. M. Cuerva, A. G. Campaña and C. Piguet, *Angew. Chem. Int. Ed.*, 2021, **60**, 10095–10102.
- 34 J.-R. Jiménez, S. Míguez-Lago, M. Poncet, Y. Ye, C. L. Ruiz, C. M. Cruz, A. G. Campaña, E. Colacio, C. Piguet and J. M. Herrera, *J. Mater. Chem. C*, 2023, **11**, 2582–2590.
- 35 O. G. Willis, F. Zinna and L. Di Bari, *Angew. Chem. Int. Ed.*, 2023, **62**, e202302358.
- 36 L. Llanos, P. Cancino, P. Mella, P. Fuentealba and D. Aravena, *Coord. Chem. Rev.*, 2024, **505**, 215675.
- 37 H.-Y. Wong, W.-S. Lo, K.-H. Yim and G.-L. Law, *Chem*, 2019, **5**, 3058–3095.
- 38 F. Zinna and L. Di Bari, *Chirality*, 2015, **27**, 1–13.
- 39 B. Doistau, J.-R. Jiménez and C. Piguet, *Front. Chem.*, , DOI:10.3389/fchem.2020.00555.
- 40 C. Förster and K. Heinze, *Chem. Soc. Rev.*, 2020, **49**, 1057–1070.
- 41 P. N. Schatz, A. J. McCaffery, W. Suetaka, G. N. Henning, A. B. Ritchie and P. J. Stephens, *J. Chem. Phys.*, 1966, **45**, 722–734.
- 42 P. J. Stephens, W. Suëtaak and P. N. Schatz, *J. Chem. Phys.*, 1966, **44**, 4592–4602.
- 43 W. R. Mason, *A practical guide to magnetic circular dichroism spectroscopy*, Wiley-Interscience, Hoboken, N.J., 2007.
- 44 F. Zinna and G. Pescitelli, *Eur. J. Org. Chem.*, 2023, **26**, e202300509.
- 45 M. Fusè, G. Mazzeo, S. Ghidinelli, A. Evidente, S. Abbate and G. Longhi, *Spectrochim. Acta A*, 2024, **319**, 124583.
- 46 J. P. Riehl and F. S. Richardson, *Chem. Rev.*, 1986, **86**, 1–16.
- 47 J. P. Riehl and F. S. Richardson, *J. Chem. Phys.*, 1977, **66**, 1988–1998.
- 48 L. D. Barron, *Molecular Light Scattering and Optical Activity*, Cambridge University Press, 2009.
- 49 P. J. Stephens, *J. Chem. Phys.*, 1970, **52**, 3489–3516.
- 50 Z. Nelson, L. Delage-Laurin and T. M. Swager, *J. Am. Chem. Soc.*, 2022, **144**, 11912–11926.
- 51 F. S. Richardson and H. G. Brittain, *J. Am. Chem. Soc.*, 1981, **103**, 18–24.
- 52 T. Wu, J. Kapitán, V. Andrushchenko and P. Bouř, *Anal. Chem.*, 2017, **89**, 5043–5049.
- 53 H. Yoshikawa, G. Nakajima, Y. Mimura, T. Kimoto, Y. Kondo, S. Suzuki, M. Fujiki and Y. Imai, *Dalton Trans.*, 2020, **49**, 9588–9594.
- 54 M. Kitahara, S. Suzuki, K. Matsudaira, S. Yagi, M. Fujiki and Y. Imai, *ChemistrySelect*, 2021, **6**, 11182–11187.
- 55 E. Krausz, G. Moran and H. Riesen, *Chem. Phys. Lett.*, 1990, **165**, 401–406.
- 56 S. Jena, S. K. Behera, J. Eyyathiyil, M. Kitahara, Y. Imai and P. Thilagar, *Adv. Opt. Mater.*, 2023, **11**, 2300923.
- 57 S. Ghidinelli, S. Abbate, G. Mazzeo, L. Paoloni, E. Viola, C. Ercolani, M. P. Donzello and G. Longhi, *Chirality*, 2020, **32**, 808–816.
- 58 S. Ghidinelli, S. Abbate, G. Mazzeo, R. Paolesse, G. Pomarico and G. Longhi, *ACS Omega*, 2021, **6**, 26659–26671.
- 59 Q. Jin, S. Chen, Y. Sang, H. Guo, S. Dong, J. Han, W. Chen, X. Yang, F. Li and P. Duan, *Chem. Commun.*, 2019, **55**, 6583–6586.
- 60 H. Toda, N. Hara, M. Fujiki and Y. Imai, *RSC Adv.*, 2021, **11**, 1581–1585.
- 61 H. Toda, S. Otake, A. Ito, M. Miyasaka, M. Fujiki and Y. Imai, *ChemPhysChem*, 2021, **22**, 2058–2062.
- 62 N. Hara, M. Kitahara, T. Sugimura, H. Toda, M. Shizuma, A. Ito, M. Miyasaka, M. Fujiki and Y. Imai, *Phys. Chem. Chem. Phys.*, 2021, **23**, 8236–8240.
- 63 R. Amasaki, M. Kitahara, T. Kimoto, M. Fujiki and Y. Imai, *Eur. J. Inorg. Chem.*, 2022, **2022**, e202101066.
- 64 T. Tomikawa, Y. Kitagawa, K. Yoshioka, K. Murata, T. Miyatake, Y. Hasegawa and K. Ishii, *J. Mater. Chem. C*, 2023, **11**, 2831–2835.
- 65 R. A. Shatwell and A. J. McCaffery, *Mol. Phys.*, 1975, **30**, 1489–1504.
- 66 A. J. McCaffery, P. Brint, R. Gale and R. A. Shatwell, *Chem. Phys. Lett.*, 1973, **22**, 600–602.
- 67 K. Murata and K. Ishii, *European Journal of Inorganic Chemistry*, 2017, **2017**, 5103–5107.
- 68 K. Ishii, J. Wada and K. Murata, *J. Phys. Chem. Lett.*, 2020, **11**, 9828–9833.
- 69 K. Hara, A. Morimoto, K. Matsudaira, S. Suzuki, S. Yagi, M. Fujiki and Y. Imai, *ChemPhotoChem*, 2022, **6**, e202100253.
- 70 T. Kuroda, M. Kitahara, S. Yagi and Y. Imai, *Front. Chem.*, , DOI:10.3389/fchem.2023.1281168.
- 71 M. Kitahara, K. Hara, S. Suzuki, H. Iwasaki, S. Yagi and Y. Imai, *Organic Electronics*, 2023, **119**, 106814.
- 72 S. Suzuki, Y. Yamamoto, M. Kitahara, R. Shikura, S. Yagi and Y. Imai, *J. Mater. Chem. C*, 2024, **12**, 3430–3436.
- 73 Y. Imai, *ChemPhotoChem*, 2021, **5**, 969–973.
- 74 S. Lenz, H. Bamberger, P. P. Hallmen, Y. Thiebes, S. Otto, K. Heinze and J. van Slageren, *Phys. Chem. Chem. Phys.*, 2019, **21**, 6976–6983.
- 75 E. I. Solomon, M. L. Neidig and G. Schenk, in *Comprehensive Coordination Chemistry II*, Elsevier, 2003, pp. 339–349.
- 76 A. Gabbani, G. Petrucci and F. Pineider, *J. Appl. Phys.*, 2021, **129**, 211101.
- 77 A. Gabbani, G. Campo, V. Bonanni, P. van Rhee, G. Bottaro, C. de Julián Fernández, V. Bello, E. Fantechi, F. Biccari, M. Gurioli, L. Armelao, C. Sangregorio, G. Mattei, P. Christianen and F. Pineider, *J. Phys. Chem. C*, 2022, **126**, 1939–1945.
- 78 A. Kamińska, A. Suchocki, S. Kobayakov, L. Arizmendi, M. Potemski and F. J. Teran, *Phys. Rev. B*, 2007, **76**, 144117.
- 79 N. F. Chilton, R. P. Anderson, L. D. Turner, A. Soncini and K. S. Murray, *J. Comput. Chem.*, 2013, **34**, 1164–1175.
- 80 J. Krzystek, A. Ozarowski and J. Telser, *Coord. Chem. Rev.*, 2006, **250**, 2308–2324.
- 81 J. Krzystek, S. A. Zvyagin, A. Ozarowski, S. Trofimenko and J. Telser, *J. Magn. Reson.*, 2006, **178**, 174–183.

Supporting information

Magnetic circularly polarized luminescence from spin flip transitions in a molecular ruby

Alessio Gabbani,^{a,b} Maxime Poncet,^c Gennaro Pescitelli,^a Laura Carbonaro,^a J. Krzystek,^d Enrique Colacio,^e Claude Piguet,^c Francesco Pineider,^{a,b} Lorenzo Di Bari,^a Juan-Ramón Jiménez*,^e Francesco Zinna*^a

^a Dipartimento di Chimica e Chimica Industriale, University of Pisa, via Moruzzi 13, 56124, Pisa, Italy

^b Department of Physics and Astronomy, University of Florence, via Sansone 1, 50019, Sesto Fiorentino, Italy

^c Department of Inorganic and Analytical Chemistry, University of Geneva, 30 quai E. Ansermet, CH-1211 Geneva 4, Switzerland

^d National High Magnetic Field Laboratory, Florida State University, Tallahassee, Florida 32310, USA

^e Departamento de Química Inorgánica, Facultad de Ciencias, Universidad de Granada and Unidad de Excelencia en Química (UEQ), Avda. Fuente Nueva s/n, 18071, Granada, Spain.

E-mail:

jrjimenez@ugr.es, francesco.zinna@unipi.it

Complex Preparation

The $[\text{Cr}(\text{dqp})_2](\text{PF}_6)_3$ (dqp = 2,6-di(quinolin-8-yl)pyridine) has been prepared according to a published method.¹

Instrumentation

MCD measurements were carried out using an in-house built, lab-scale instrument equipped with a 1.4 T electromagnet. Light emitted by a 300 W Xe arc lamp (Newport) is monochromated (Newport Oriel Cornerstone 260) and chopped at 440 Hz. Polarization modulation at 47 kHz between LCP and RCP is obtained with a Glan-Thompson polarizer coupled to a photoelastic modulator (Hinds Instruments PEM 100) set to $\lambda/4$ retardation. The beam is then directed through the bore of an electromagnet (Buckley Systems Ltd. GMW model 3470) where the sample is placed. Light is collected by a photomultiplier tube (Hamamatsu R376). After transimpedance amplification, the output voltage of the detector is fed to two lock-in amplifiers, one referenced to the polarization modulation frequency (Stanford Research Systems SR850) and one to the light chopping frequency (Signal Recovery 7280); the ratio of the two signals is taken as the differential absorption (dichroism) ΔA . MCD signal is then obtained by the semi difference between the signals obtained at +1.4 T and -1.4 T. Calibration of the MCD signal is carried out against an aqueous solution of $[\text{Fe}(\text{CN})_6]^{3+}$ of known concentration. The MCD spectra of the Cr^{3+} complex were recorded in CH_3CN solution in a 1 mm optical path cuvette. The concentration was $1.67 \cdot 10^{-4}$ M and $2.57 \cdot 10^{-2}$ M for the high and low energy region respectively. Given the slits used (0.6 mm) and the grating employed in the monochromator, the spectral resolution was 1.9 nm. MCD vs field plots in the +1.4/-1.4 T range were also acquired by regulating the current passing in the coils of the electromagnet. The strength of the magnetic field was measured with a Hall probe.

MCPL measurements were carried out with an in-house built set-up mounted on an open optical bench (Figure S1). The sample is placed in front of 0.4 T NdFeB permanent magnet, and it is excited with a 365 nm LED (M365D1, Thorlabs) with a 0° geometry, using a dichroic mirror (cutoff 400 nm). The collected light is passed through a photoelastic modulator (Hinds Instruments PEM 100) set to $\lambda/4$ retardation modulated at 50 kHz, coupled with a Glan-Thompson polarizer. Ambient light is filtered out using a chopper. The light emitted by the sample then passes through a monochromator (Oriel Cornerstone 130) and is detected by a mutlialkali photomultiplier tube (Hamamatsu R376). The monochromator slits were set to 0.7 mm (spectral resolution of 9 nm), as this was found to be a good compromise between having enough light at the detector while ensuring enough spectral resolution to distinguish the two SF transitions (Figure S1). The voltage of the photomultiplier tube used was 650 V. After transimpedance amplification, the output voltage of the detector is fed to two lock-in amplifiers, one referenced to the polarization modulation frequency (MFLI, Zurich Instruments) and one to the light chopping frequency (Stanford Research Systems SR850). The PL and MCPL spectra are acquired simultaneously by using a LabVIEW routine. The spectra were recorded in a 2 mM CH_3CN solution, in Ar atmosphere, using a rotaflow 1 mm cuvette and deaerated CH_3CN as solvent. 9 spectra for each field (+0.4 and -0.4 T) were acquired and averaged. The excitation LED was powered with a current of 250 mA. The resulting excitation optical power was 48 mW, as measured with a power meter.

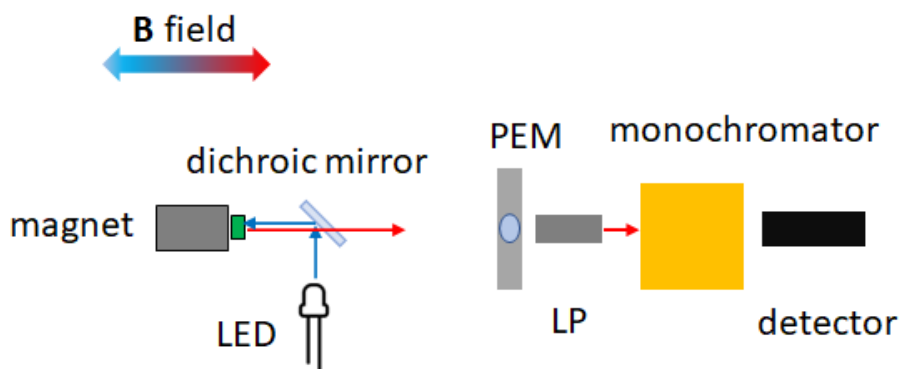


Figure S1. Simplified scheme of the set up employed for MCPL measurements.

High-frequency and -field EPR (HFEPR) spectra were recorded at the National High Magnetic Field Laboratory on 49 mg of polycrystalline sample either loose (unconstrained) or pressed into a pellet with *n*-eicosane. A homodyne spectrometer at the EMR Facility associated with a 15/17-T superconducting magnet is described in bibliography² with a modification of using a Virginia Diodes (VDI, Charlottesville, VA, USA) chain operating in the 48 – 540 GHz frequency range. Detection was provided with an InSb hot electron bolometer (QMC Ltd., Cardiff, UK). The magnetic field was modulated at 50 kHz for detection purposes. A Stanford Research Systems SR830 lock-in amplifier converted the modulated signal to *dc* voltage.

Variable-temperature (2–300 K) magnetic susceptibility measurements were carried out on polycrystalline samples under an applied field of 0.3 T using a DynaCool PPMS-9 physical measurement equipment. The magnetic susceptibility values were corrected from the diamagnetism of the molecular constituents and of the sample holder.

Additional figures

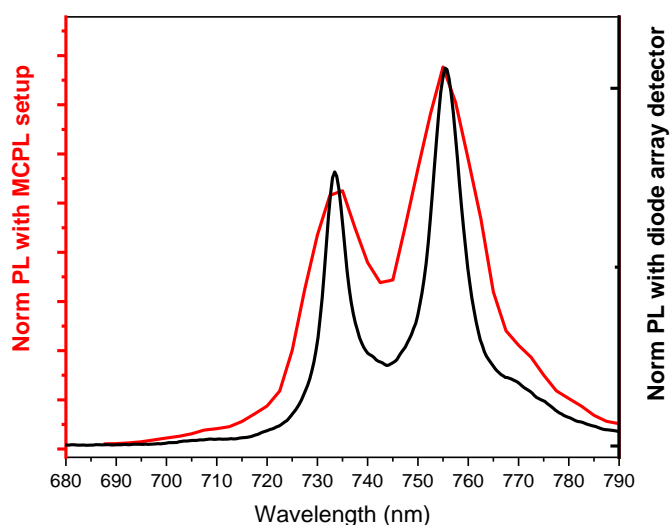


Figure S2: Comparison between the PL measured with the MCPL setup with a spectral resolution of 9 nm, and the one measured with an array detector having 2 nm of spectral resolution (Optosky ATP2000P Modular spectrometer, Crisel Instruments).

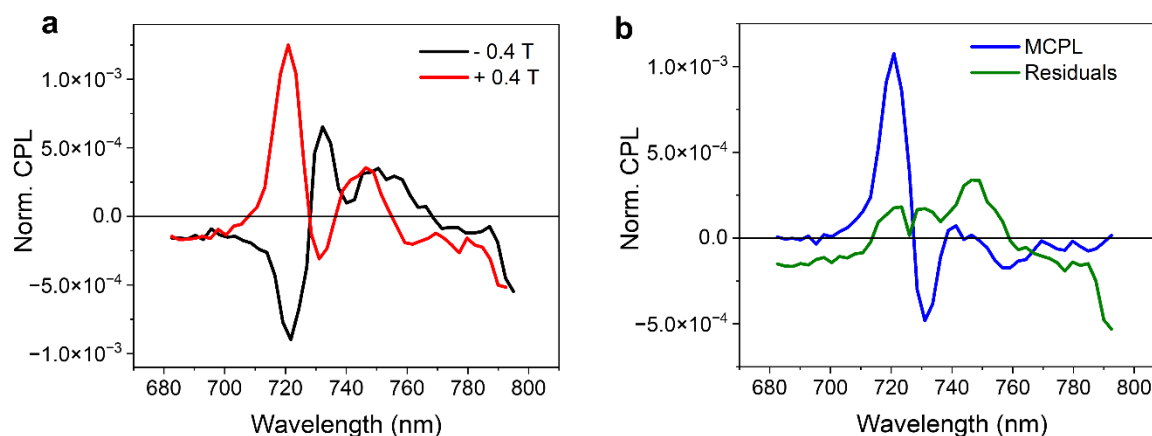


Figure S3. a. Normalized MCPL signals under ± 0.4 T; **b.** MCPL spectrum obtained by the semi-difference of the signals in **a** (see eq. 2 in the text), and the residuals obtained as the semi-sum of the signals.

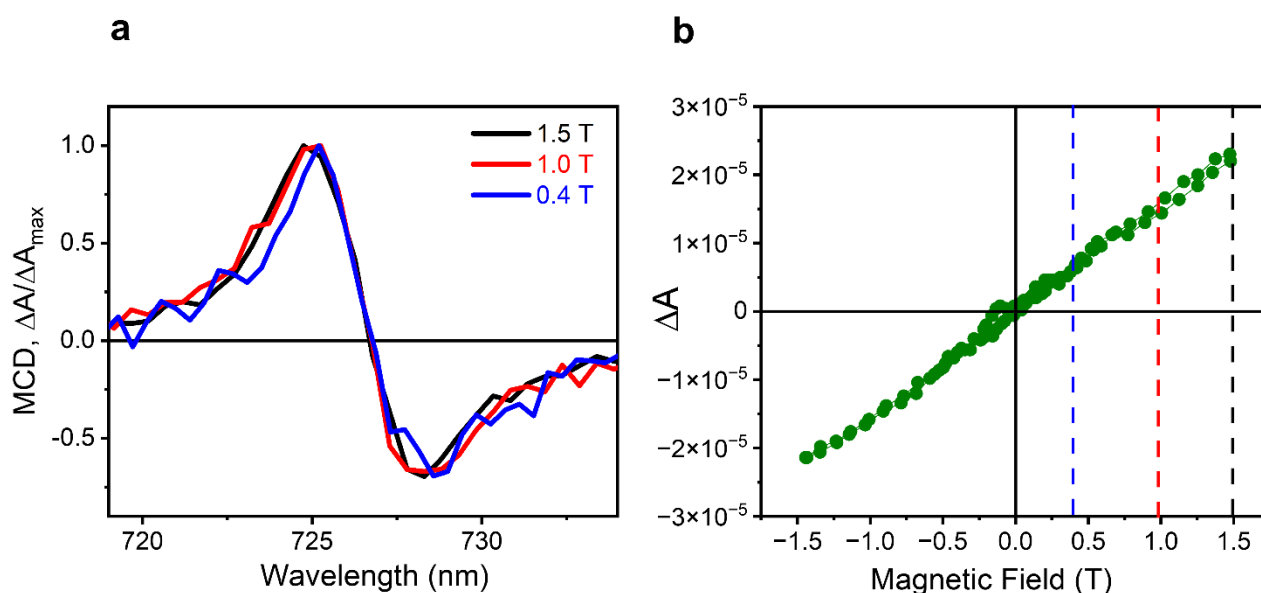


Figure S4. a. MCD spectrum of the most intense the spin-flip transition at different applied magnetic fields; **b.** MCD signal at 725 nm as a function of the applied magnetic field. The vertical lines in **b** show the applied field used to acquire the spectra in **a**.

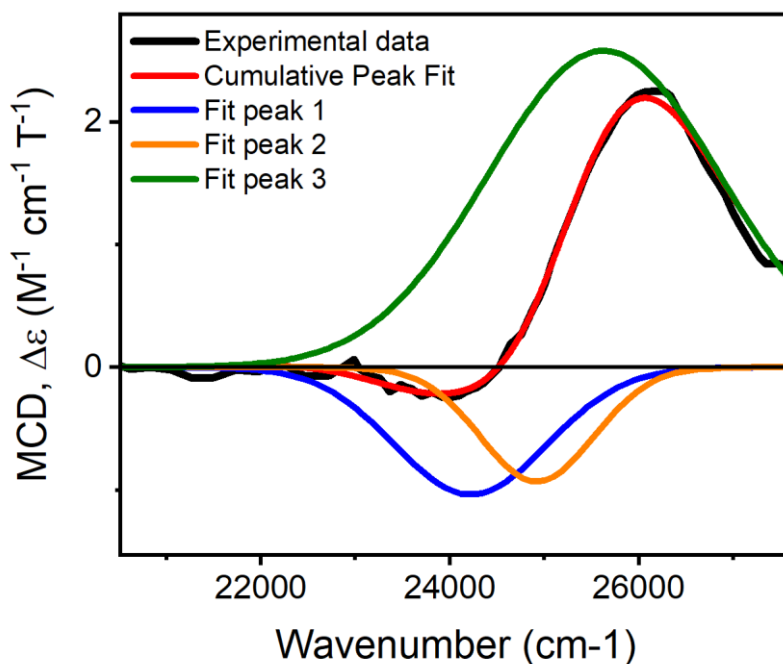


Figure S5. Phenomenological fitting of the low energy tail of the MCD spectrum.

Table S1. Values obtained from the fitting of the low energy tail of the MCD spectrum.

	Parameter ^a	Value	Standard Error
Peak 1	E	24220 cm ⁻¹	3112 cm ⁻¹
	A	-838	13
	σ	809 cm ⁻¹	1186 cm ⁻¹
Peak 2	E	24922 cm ⁻¹	356 cm ⁻¹
	A	-559	15
	σ	601 cm ⁻¹	394 cm ⁻¹
Peak 3	E	25630 cm ⁻¹	795 cm ⁻¹
	A	3175	19
	σ	1228 cm ⁻¹	271 cm ⁻¹

^a E = energy, A = area of the Gaussian, σ = peak full width at half maximum.

According to Lenz *et al.*³, in a D_2 geometry, the zero-field parameters D and E can be calculated taking into account the energies ΔE_i of the 3 components of the $^4A_2 \rightarrow ^4T_2$ transitions (with $\Delta E_3 > \Delta E_2 > \Delta E_1$):

$$D = \frac{1}{2} \zeta^2 \left(\frac{8}{\Delta E_1} - \frac{4}{\Delta E_2} - \frac{4}{\Delta E_3} \right) \quad (\text{eq S1})$$

$$E = \frac{1}{2} \zeta^2 \left(\frac{4}{\Delta E_2} - \frac{4}{\Delta E_3} \right) \quad (\text{eq S2})$$

Where ζ is spin-orbit coupling constant of the free Cr(III) ion (273 cm^{-1}).⁴ The ZFS can be calculated as:

$$\text{ZFS} = 2\sqrt{D^2 + 3E^2} \quad (\text{eq S3})$$

Analysis of MCPL data

According to the rigid shift model, the MCPL can be modelled by two equal, but opposite, bell-shaped functions displaced by the Zeeman splitting (Z), with respect to the barycenter energy (E). Such functions share the same parameters with the one used to fit the photoluminescence band (with the same bandwidth σ , peak area, etc.) and are obtained by simultaneously fitting the MCPL and the PL (Figure S6).

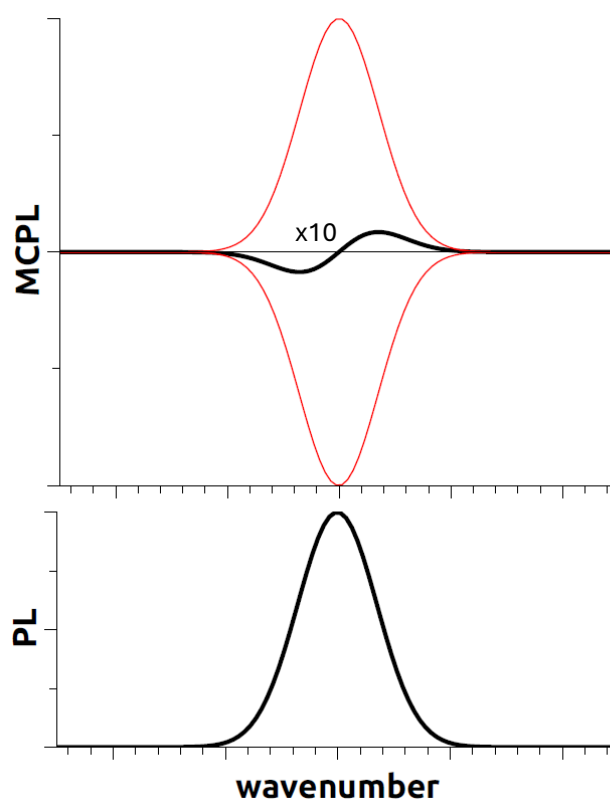


Figure S6. Illustrative example of the rigid-shift approximation applied to MCPL. The derivative shape (amplified 10 times for the sake of visualization) emerges from the partial cancellation of two opposite sign identical Gaussian functions translated by a dx (here $\sigma/dx = 100$)

Fitting functions

We chose pseudo-Voigt line shapes (eq S12) to fit the PL spectra, one for each of the two emissive transitions.

$$PL_i = A_i \left[\mu_i \frac{2}{\pi} \frac{\sigma_i}{4(x-E_i)^2 + \sigma_i^2} + (1 - \mu_i) \frac{\sqrt{4\log 2}}{\sqrt{\pi}\sigma_i} \exp\left(\frac{-4\log 2 \cdot (x-E_i)^2}{\sigma_i^2}\right) \right] \quad (\text{eq S4})$$

With $i = 1, 2$, where A_i is the peak Area, σ_i the full width at half maximum, E_i is the energy centre of the PL peak, while μ_i is a shape parameter with values in the range from 0 to 1, with 1 representing a pure Lorentzian shape and 0 a pure Gaussian shape.

MCPL of each SF transition is modelled as the difference between two sets of peak functions (two positive and two negative) with the same parameters used in equation S12 to fit the PL spectrum, but shifted in energy by a factor ΔE_i . Each fitting function used to model MCPL is therefore:

$$MCPL_i = \pm \frac{1}{2} (A_i \pm dA_i) \left[\mu_i \frac{2}{\pi} \frac{\sigma_i}{4(x - E_i - \Delta E_i)^2 + \sigma_i^2} + (1 - \mu_i) \frac{\sqrt{4 \log 2}}{\sqrt{\pi} \sigma_i} \exp \left(\frac{-4 \log 2 \cdot (x - E_i - \Delta E_i)^2}{\sigma_i^2} \right) \right] \quad (\text{eq S5})$$

where dA_i is added as an empirical parameter accounting for the slight asymmetry of the MCPL derivative-like signal. ΔE_i is expressed using the energy of the ground state sublevels found through HFEPR analysis. In particular, for the 4 transitions depicted in Figure 4 (main text), ΔE_i is reduced to the following expressions for $i = 1 - 4$:

$$|+1/2\rangle \rightarrow |-1/2\rangle: \quad \Delta E_1 = +\frac{Z}{2} - 0.44 \text{ cm}^{-1} \quad (\text{eq S6})$$

$$|-1/2\rangle \rightarrow |-3/2\rangle: \quad \Delta E_2 = -\frac{Z}{2} + 1.03 \text{ cm}^{-1} \quad (\text{eq S7})$$

$$|-1/2\rangle \rightarrow |+1/2\rangle: \quad \Delta E_3 = -\frac{Z}{2} - 0.66 \text{ cm}^{-1} \quad (\text{eq S8})$$

$$|+1/2\rangle \rightarrow |+3/2\rangle: \quad \Delta E_4 = +\frac{Z}{2} + 0.07 \text{ cm}^{-1} \quad (\text{eq S9}),$$

Where Z is considered as: $Z = \mu_B g H \Delta M_s = 0.36 \text{ cm}^{-1}$ (μ_B is the Bohr magneton and g the electron g -factor), for 0.4 T of applied field and $\Delta M_s = 1$, and is thus kept as a fixed parameter during the fitting. Note that the transitions associated to the energies in eq. give a positive sign contribution to MCPL, while those associated to eq. give a negative contribution (compare with Figure 4).

As it is very weak, in first approximation we neglect the low energy transition in the MCPL fitting functions.

Thus, equations S4 and S5 are used to fit simultaneously the PL and MCPL spectra, using a home-built matlab routine. In Figure S7 we show the fitting using different peak functions: Gaussian, Lorentz or Pseudo-Voigt functions, which is a linear combination of the first two functions. The parameters extracted from the fitting are reported in Table S2. We also report a fitting without the empirical parameter dA ($dA = 0$). The parameters obtained through the fitting are reported in Table S2. The pseudoVoigt function retraces better the PL and MCPL line shape, revealing a reasonable agreement with the experimental data, despite the significant approximation made in defining the fitting functions. On the other hand, similar line shapes are obtained with different peak functions, indicating the robustness of the fitting procedure.

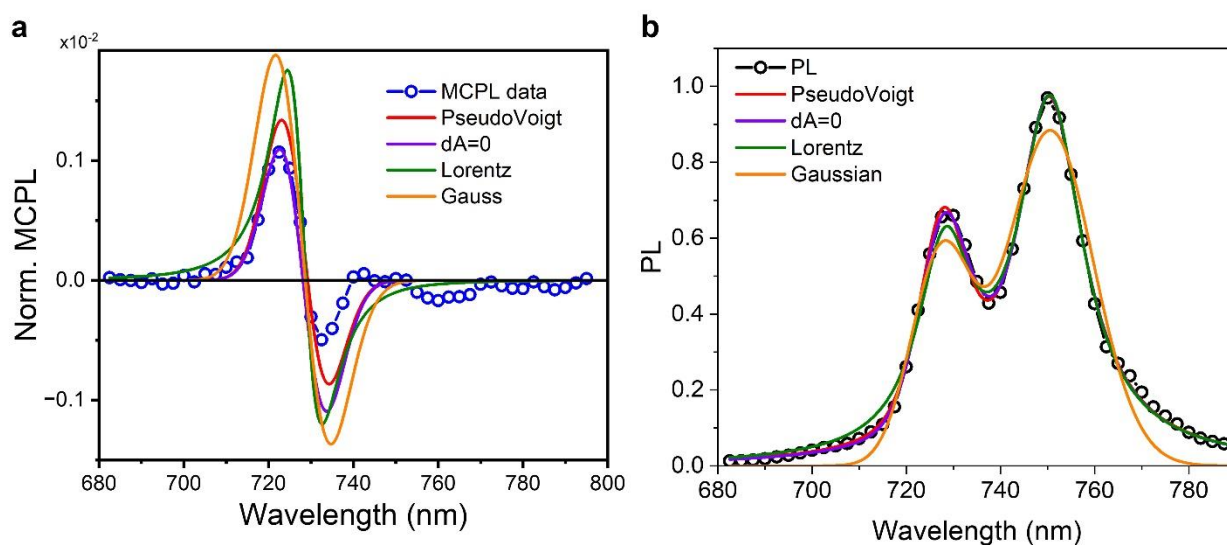


Figure S7. Fitting of normalized MCPL (a) and PL (b) spectra with different peak functions.

Table S2. Parameters extracted from MCPL and PL fitting of the high energy transition using equations S12-S13.

	High energy transition					Low energy transition			
	A	σ (cm ⁻¹)	E (cm ⁻¹)	μ	dA	A	σ (cm ⁻¹)	E (cm ⁻¹)	μ
Pseudo-Voigt function									
Param	0.011	247	13733	0.02	$1.2 \cdot 10^{-5}$	0.058	310	13324	1.00
Error	0.003	12	5	0.50	$0.6 \cdot 10^{-5}$	0.002	13	4	0.07
dA fixed to 0									
Param	0.011	247	13732	0.02	0*	0.058	309	13324	1.00
Error	0.004	14	5	0.54	-	0.002	15	4	0.08
Lorentz function ($\mu=1$)									
Param	0.027	266	13729	1*	$1.9 \cdot 10^{-5}$	0.054	299	13320	1*
Error	0.006	29	11	-	$1.4 \cdot 10^{-5}$	0.004	20	6	-
Gaussian function ($\mu=0$)									
Param	0.022	291	13740	0*	$1.6 \cdot 10^{-5}$	0.044	373	13319	0*
Error	0.010	44	32	-	$2.2 \cdot 10^{-5}$	0.006	41	16	-

* this parameter is kept fixed during the fitting

DC magnetometry

The *dc* magnetic properties of $[\text{Cr}(\text{dqp})_2](\text{PF}_6)_3$ were studied in the 2–300 K temperature range with an applied magnetic field of 1000 Oe. The $\chi_M T$ vs T curve (χ_M is the molar magnetic susceptibility) is shown in Figure S7. The $\chi_M T$ value at room temperature of $1.90 \text{ cm}^3 \text{ mol}^{-1} \text{ K}$ is very close to expected value of $1.875 \text{ cm}^3 \text{ mol}^{-1} \text{ K}$ for a Cr(III) ion with $S = 3/2$ if $g = 2$, which agrees with a quartet ground state (4A_2). Upon cooling, the $\chi_M T$ product remains almost constant until about 10 K and then sharply decreases to reach a value of $1.78 \text{ cm}^3 \text{ mol}^{-1} \text{ K}$ at 2 K.

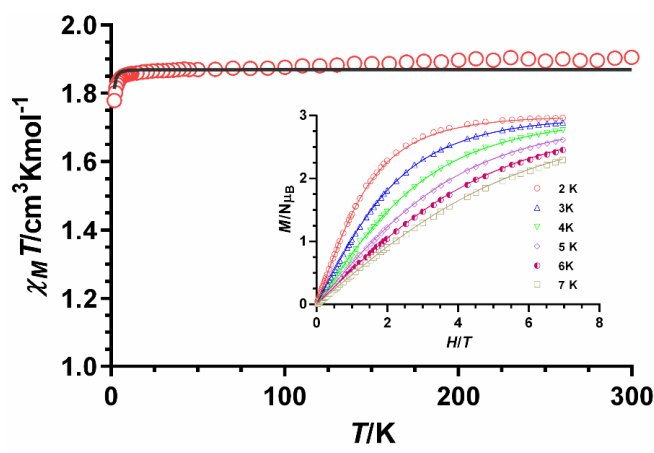


Figure S8. Temperature dependence of χ_{MT} (red circles) and field dependence of the magnetization at 2–7 K (inset). Solid lines represent the best fit to equation.

The field dependence of the magnetization of the Cr(III) compound in the 2–7 K temperature range and magnetic fields ranging from 0 to 7 T have been studied (Figure S7 inset). The magnetization values at 2 K and under the maximum applied field of 7 T of $2.97 N\beta$ match well with the theoretical saturation value of $3 N\beta$ expected for an isolated Cr(III) ion with $g = 2$ and $S = 3/2$.

The magnetic susceptibility and magnetization data were simultaneously fitted using the PHI program⁵ with the ZFS spin Hamiltonian shown in equation 1.

$$\hat{H} = D[\hat{S}_z^2 - S(S+1)/3] + E(\hat{S}_x^2 - \hat{S}_y^2) + \mu_B \sum_{i=x,y,z} g_i \vec{H}_i \hat{S}_i \quad (\text{eq S10})$$

where the first and second terms account the axial and rhombic magnetic anisotropies, respectively, and the third term represents the Zeeman interaction. To improve the fit of the data and to avoid over-parameterization a term corresponding to the temperature independent paramagnetism (TIP) was included in the above Hamiltonian. It is worth noting that the low accuracy of the magnetic measurements for determining E and $|E/D|$ parameters prevent extracting very reliable ZFS parameters for the Cr(III) compound, particularly the sign of D (the fit of the data is the same with positive and negative D values) and the magnitude of E . In view of these considerations, E was fixed to zero in the fitting procedure. The best fit led to the following magnetic parameters: $|D| = 0.72 \text{ cm}^{-1}$, $g = 1.99$, $\text{TIP} = 0.165 \times 10^{-3} \text{ cm}^3 \text{ mol}^{-1}$ and $R = 2.5 \times 10^{-7}$. It is worth remarking that that magnitude of the D value extracted from the *dc* magnetic data of the compound is very similar to those experimentally and theoretically found for other Cr(III) complexes with slightly distorted octahedral coordination.^{6,7}

HFEPR

HFEPR data analysis and simulation was accomplished using a software package SPIN by A. Ozarowski, freely available at: <https://osf.io/z72tg/>. The same software has a very useful option to calculate the mixing coefficients of the spin sublevels, and their corresponding energies, which is achieved by diagonalizing the spin Hamiltonian matrix containing the ZFS and Zeeman terms. The results of this procedure are shown in Tables S3 and S4.

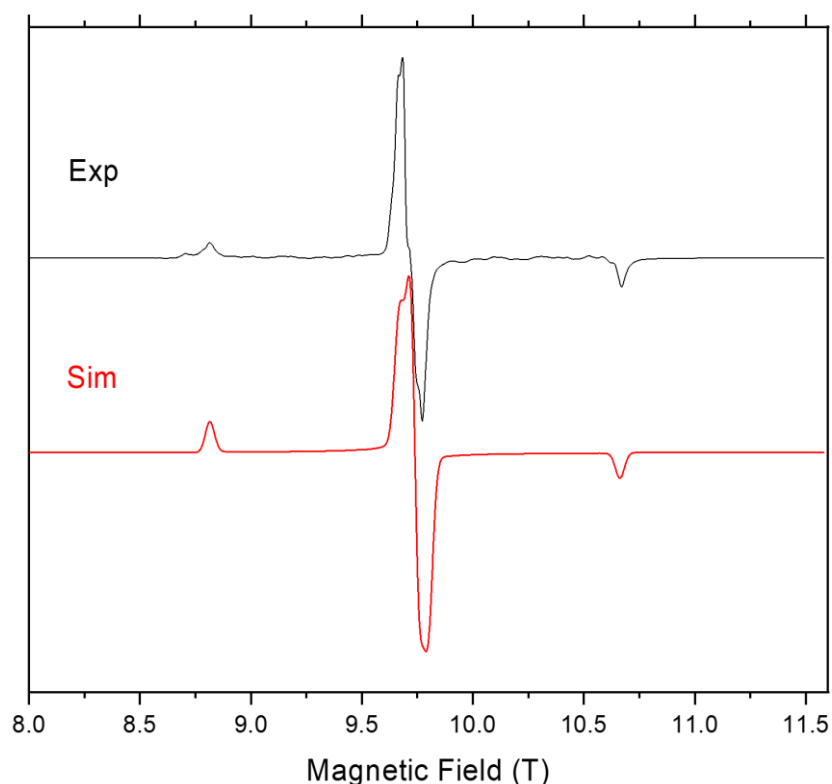


Figure S9. The allowed transitions in the EPR spectrum of $[\text{Cr}(\text{dqp})_2](\text{PF}_6)_3$ constrained as a pellet at 10 K and 270 GHz (black trace) accompanied by their simulation (red trace) using the following spin Hamiltonian parameters: $S = 3/2$, $D = 0.43 \text{ cm}^{-1}$, $E = 0.14 \text{ cm}^{-1}$ ($E/D = 0.325$), $g_x = 1.99$, $g_{y,z} = 1.98$. The simulation assumed a perfectly random orientation of the crystallites in space. The poorly resolved structure on the central line is due to either a deviation from the maximum rhombicity condition ($E/D < 0.33$) or slight g -anisotropy or both.

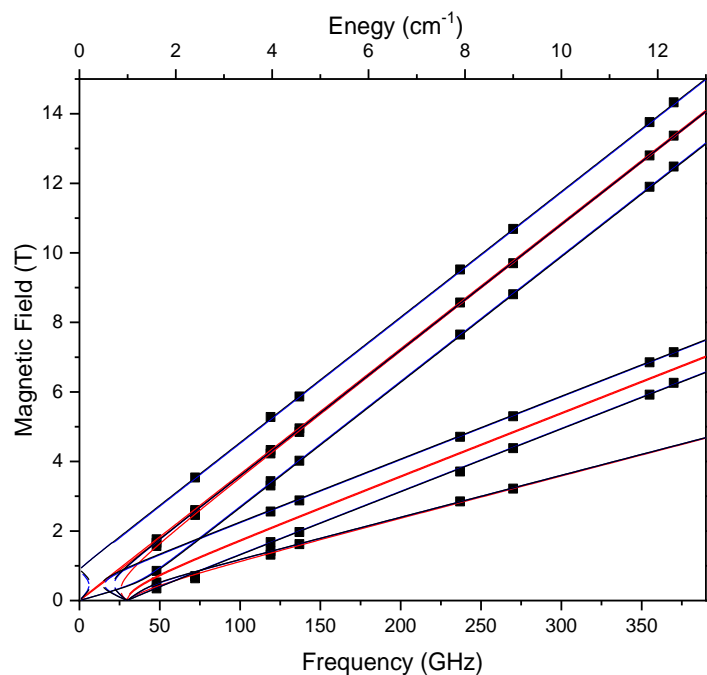


Figure S10. Field vs. frequency map of turning points (squares) in the EPR spectra accompanied by its simulations (curves) using the following best-fitted spin Hamiltonian parameters: $S = 3/2$, $D = -0.436 \text{ cm}^{-1}$, $E = -0.134 \text{ cm}^{-1}$ ($E/D = 0.309$), $g_{iso} = 1.980$. Red curves: magnetic field B_0 parallel to the x-axis of the ZFS tensor; blue: $B_0 \parallel y$; blue: $B_0 \parallel z$.

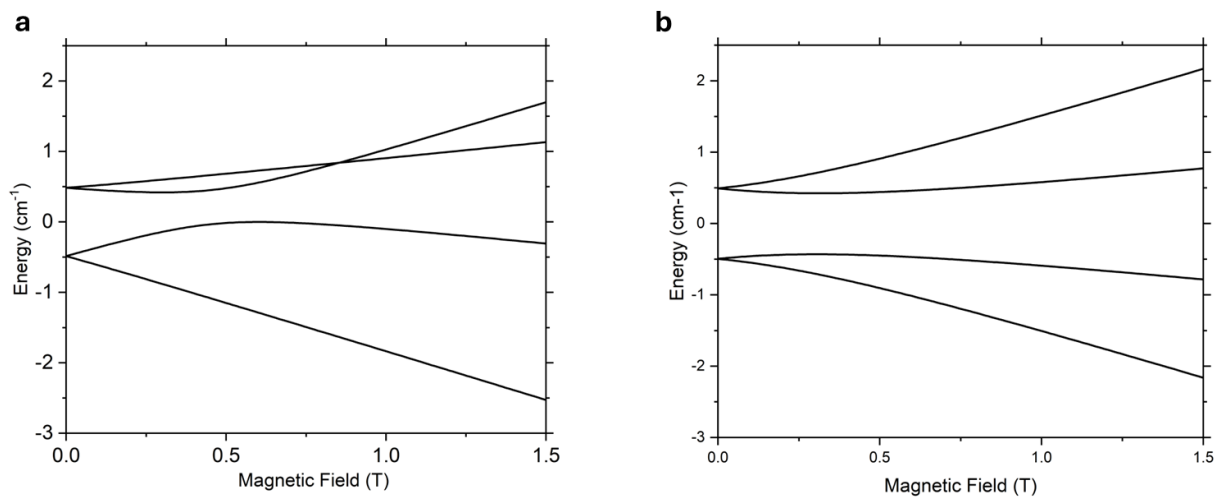


Figure S11. Representation of the HFEPR ground state energy levels for a $S = 3/2$ spin state for the low field region. a: $B_0 \parallel z$, b: $B_0 \parallel x$ (for $B_0 \parallel y$ an almost equivalent situation to case a is obtained, albeit with an inverted level energy order).

Table S3. Energy levels of the spin sublevels of the 4A_2 ground state at 0.4 T (0 is the energy of the unsplit 4A_2 state) and mixing coefficients squared for $B_0 || z$ (an almost equivalent situation is obtained for $B_0 || y$). The first column indicates the main character of the state.

Mixed state	Energy / cm^{-1}	+3/2	+1/2	-1/2	-3/2
$ \widetilde{+1/2}\rangle$	0.66026	0.00000	0.97784	0.00000	0.02215
$ \widetilde{-1/2}\rangle$	0.44380	0.37843	0.00000	0.62157	0.00000
$ \widetilde{+3/2}\rangle$	-0.07031	0.62157	0.00000	0.37843	0.00000
$ \widetilde{-3/2}\rangle$	-1.03375	0.00000	0.022156	0.00000	0.97784

Table S4. Energy levels of the spin sublevels of the 4A_2 ground state at 0.4 T (0 is the energy of the unsplit 4A_2 state) and mixing coefficients squared for $B_0 || x$. The first column indicates the main character of the state.

Mixed state	Energy / cm^{-1}	+3/2	+1/2	-1/2	-3/2
$ \pm 1/2\rangle$	0.81387	0.00175	0.49825	0.49825	0.00175
$ \pm 1/2\rangle$	0.43793	0.15025	0.34975	0.34975	0.15025
$ \pm 3/2\rangle$	-0.44038	0.49825	0.00175	0.00175	0.49825
$ \pm 3/2\rangle$	-0.81142	0.34975	0.15025	0.15025	0.34975

Note that at high magnetic field the mixing is negligible and the order (from high to low energy) of the states is $|+3/2\rangle$, $|+1/2\rangle$, $|-1/2\rangle$, $|-3/2\rangle$.

References

- 1 J.-R. Jiménez, B. Doistau, C. M. Cruz, C. Besnard, J. M. Cuerva, A. G. Campaña and C. Piguet, *J. Am. Chem. Soc.*, 2019, **141**, 13244–13252.
- 2 A. K. Hassan, L. A. Pardi, J. Krzystek, A. Sienkiewicz, P. Goy, M. Rohrer and L.-C. Brunel, *J. Magn. Reson.*, 2000, **142**, 300–312.
- 3 S. Lenz, H. Bamberger, P. P. Hallmen, Y. Thiebes, S. Otto, K. Heinze and J. van Slageren, *Phys. Chem. Chem. Phys.*, 2019, **21**, 6976–6983.
- 4 P. E. Hoggard, *Zeitschrift für Naturforschung A*, 1981, **36**, 1276–1288.
- 5 N. F. Chilton, R. P. Anderson, L. D. Turner, A. Soncini and K. S. Murray, *J. Comput. Chem.*, 2013, **34**, 1164–1175.
- 6 G. Elbers, S. Remme and G. Lehmann, *Inorg. Chem.*, 1986, **25**, 896–897.
- 7 D. G. Liakos, D. Ganyushin and F. Neese, *Inorg. Chem.*, 2009, **48**, 10572–10580.